Thermal dielectron measurements with the STAR experiment

Chenliang Jin
Stony Brook University
04/02/2026


Stony Brook, NY
(Long Island)
~1,630 mi
Houston, TX
Houston, TX
Stony Brook, NY

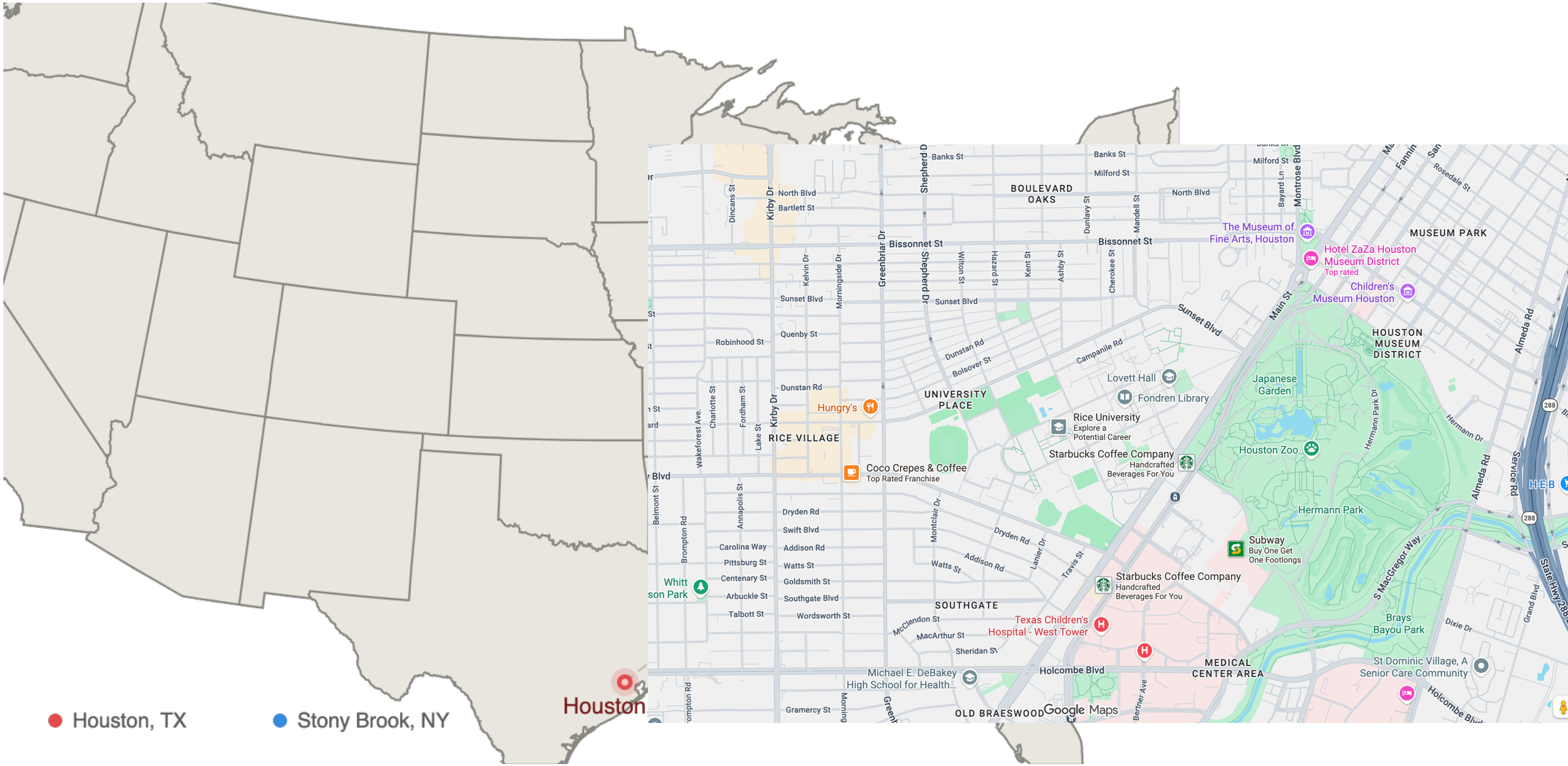
Houston, TX
Stony Brook, NY
Houston
Banks St
Milford St
BOULEVARD OAKS
North Blvd
Bartlett St
Bissonnet St
Sunset Blvd
Quenby St
Robinhood St
Dunstan Rd
Bolsover St
Campanile Rd
UNIVERSITY PLACE
RICE VILLAGE
Hungry's
Coco Crepes & Coffee
Top Rated Franchise
Dryden Rd
Swift Blvd
Addison Rd
Watts St
Goldsmith St
Southgate Blvd
Wordsworth St
SOUTHGATE
Carolina Way
Pittsburg St
Centenary St
Arbuckle St
Talbott St
Whitt son Park
Gramercy St
OLD BRAESWOOD
Michael E. DeBakey High School for Health...
Holcombe Blvd
MEDICAL CENTER AREA
Texas Children's Hospital - West Tower
McClendon St
MacArthur St
Sheridan St
Starbucks Coffee Company
Handcrafted Beverages For You
Subway
Buy One Get One Footlongs
Hermann Park
Brays Bayou Park
St Dominic Village, A Senior Care Community
Lovett Hall
Fondren Library
Rice University
Explore a Potential Career
Starbucks Coffee Company
Handcrafted Beverages For You
Houston Zoo
Japanese Garden
HOUSTON MUSEUM DISTRICT
MUSEUM PARK
The Museum of Fine Arts, Houston
Hotel ZaZa Houston Museum District
Top rated
Children's Museum Houston
Google Maps

Outline

- QCD Phase Diagram and Heavy-ion collision
- Dileptons as probe
- Experimental setup in STAR
- Dielectron analysis at RHIC BES-II energies
  - Spectrometer, Thermometer
- Dielectron physics in the future
- Summary and Outlook

QCD Phase Diagram

- Hadronic phase: quarks are confined within hadrons.
- Quark-Gluon Plasma (QGP) phase:
  - Deconfined quarks and gluons.
  - Local thermal equilibrium.
- Hadronization: Phase transition (PT) to the Hadron Gas phase.
- First/second order phase transition or Crossover?
- Existence of Critical Point (CP)?

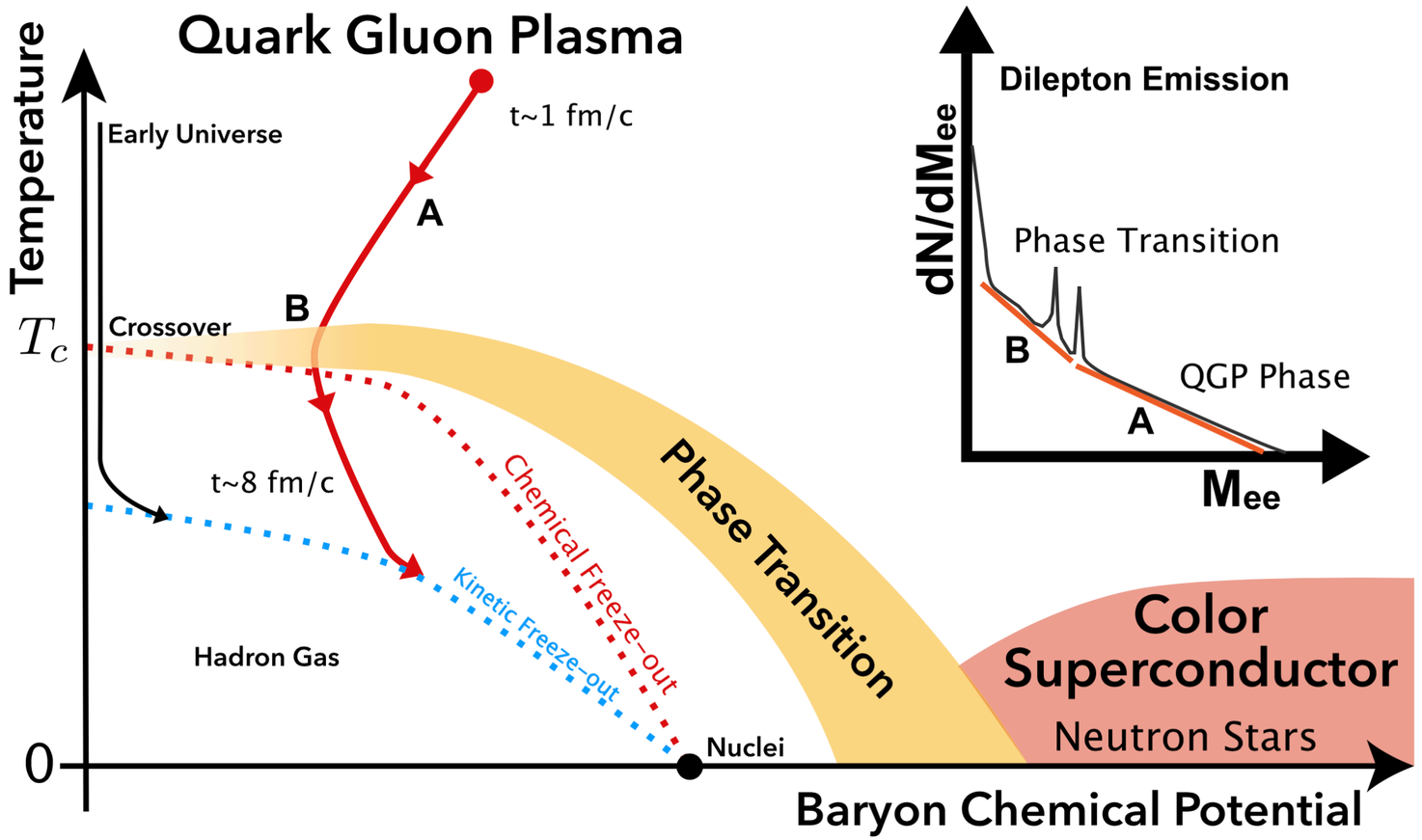

Charting QCD Phase Diagram

- Experimentally, one can access different regions of phase diagram by varying centre-of-mass energy of colliding ions.
  - Current experiment data already cover around 4 orders of magnitude.

- Low μ_B region: LHC, RHIC, FAIR

- Higher μ_B region: discovery potential with possible 1st order PT and a conjectured CP.
  - HADES, RHIC beam energy scan (BES: this thesis)
  - CBM, NA60+ in the future

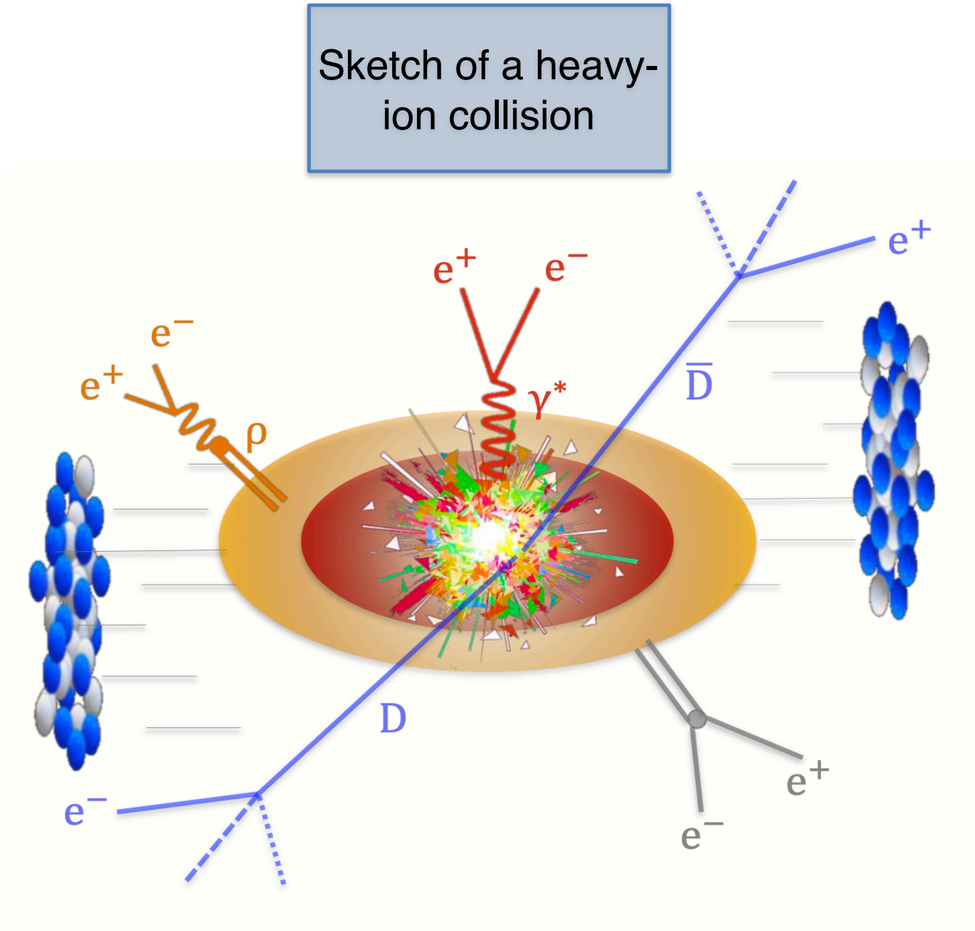

Jerome Jung, EP Seminar CERN, 2024

Relativistic Heavy-ion Collision Evolution

- Initial state & pre-equilibrium.
- QGP fireball expansion: Hydrodynamic evolution.
- Hadronization: Different possible phase transition.
- Chemical freeze-out: Ceasing inelastic scattering processes.
- Kinetic freeze-out: Ceasing elastic scattering processes.

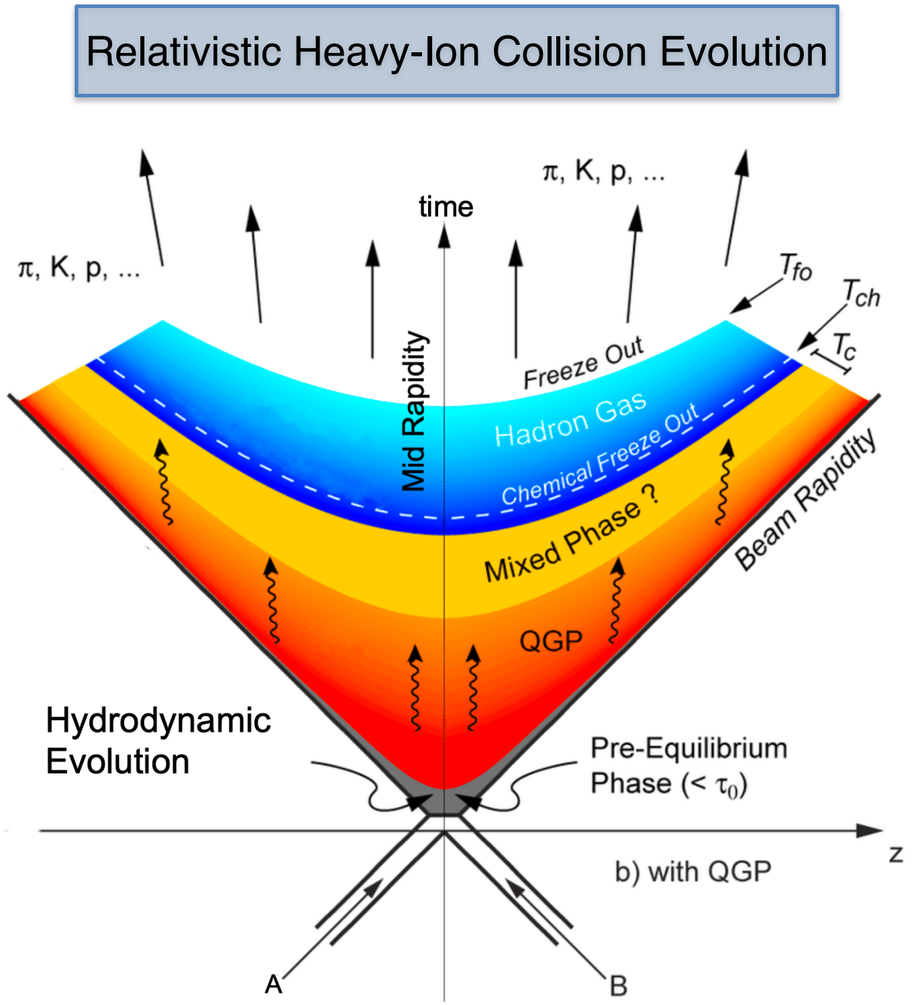

Why Dileptons?

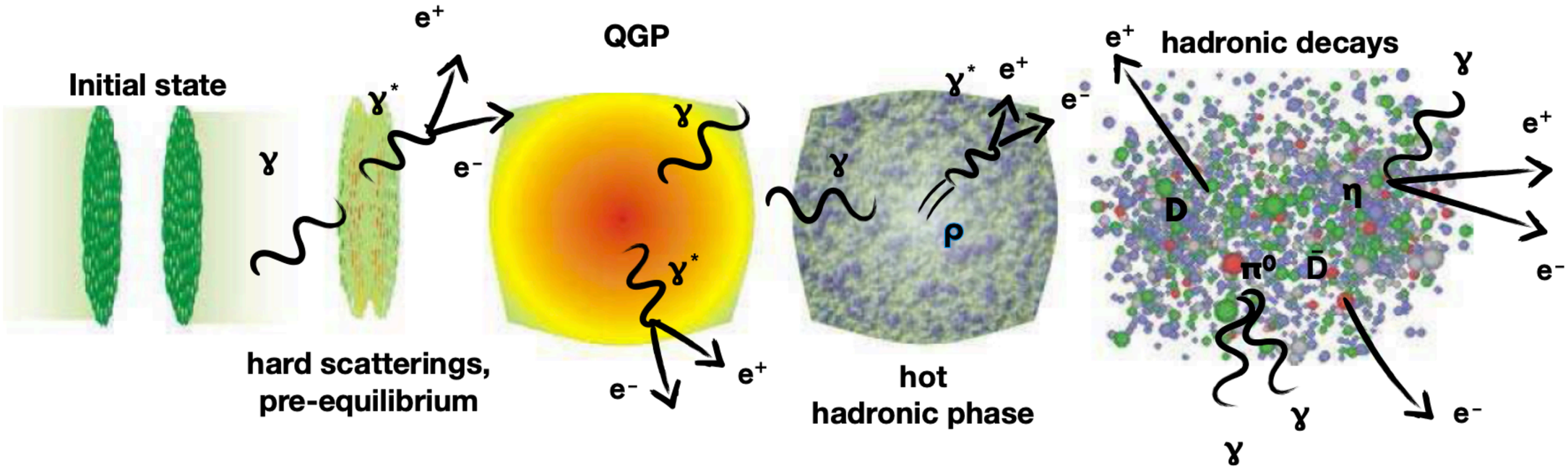

- EM probes are penetrating:
  - No coupling to strongly interacting matter.
  - Mean free path length ≫ size of the fireball.
  - Reflect the whole history of a collision.
- Dileptons vs. direct photon: encode additional information: invariant mass.
  - No blue-shift effect.

Dielectron invariant mass spectrum

- Composition of the dielectron spectrum:
  ➡Seperation via invariant mass.

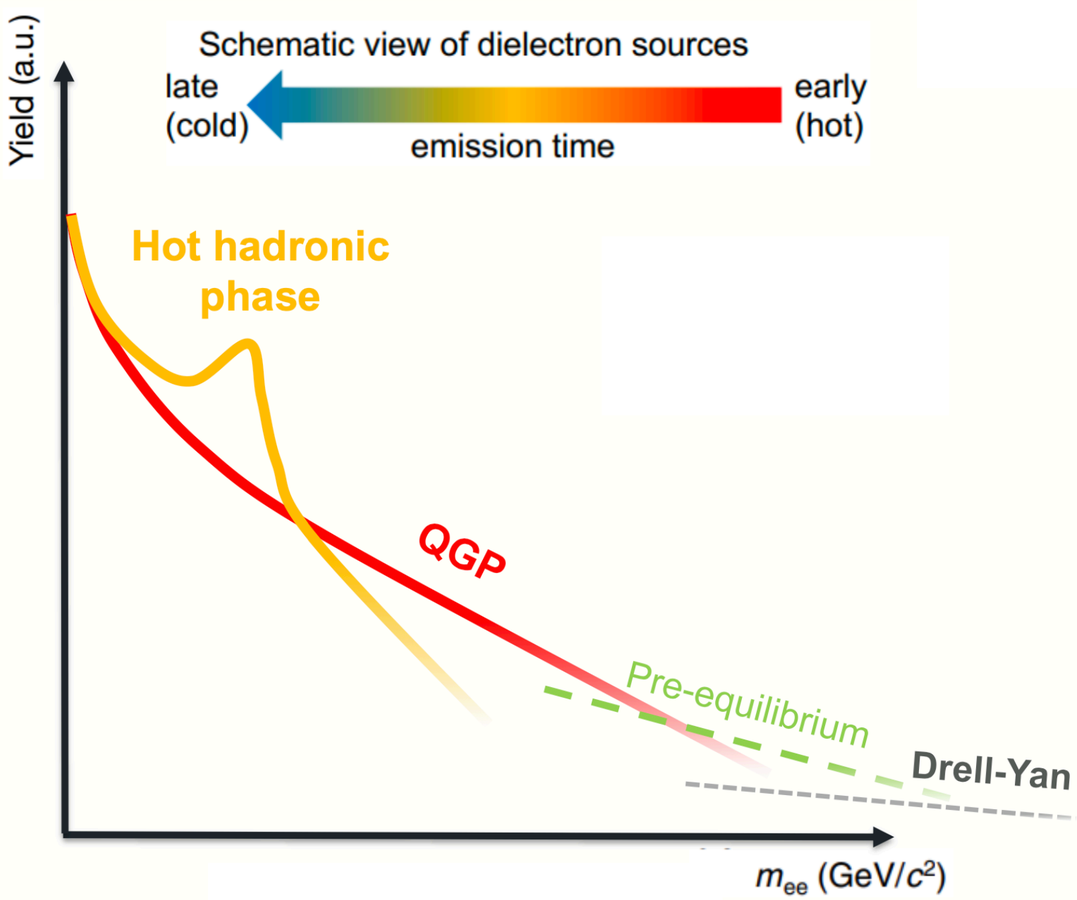

Jerome Jung, EP Seminar CERN, 2024

Dielectron invariant mass spectrum

- High Mass Range (HMR: $M_{ee} > 3$ GeV/c²)
  - Drell-Yan: $q\bar{q} \rightarrow \gamma^* \rightarrow e^+e^-$
  - Heavy quarkonia: *J/ψ* and ϒ.

- Intermediate Mass Range (IMR: $1 < M_{ee} < 3$ GeV/c²)
  - QGP thermal radiation: $q\bar{q} \rightarrow e^+e^-$
  - Semi-leptonic decay of correlated charm: $c\bar{c} \rightarrow e^+e^-X$

- Low Mass Range (LMR: $M_{ee} < 1$ GeV/c²)
  - In-medium vector mesons.
  - Light meson decays: *π*, *η* Dalitz decays.
  - Transport coefficients (electrical conductivity).

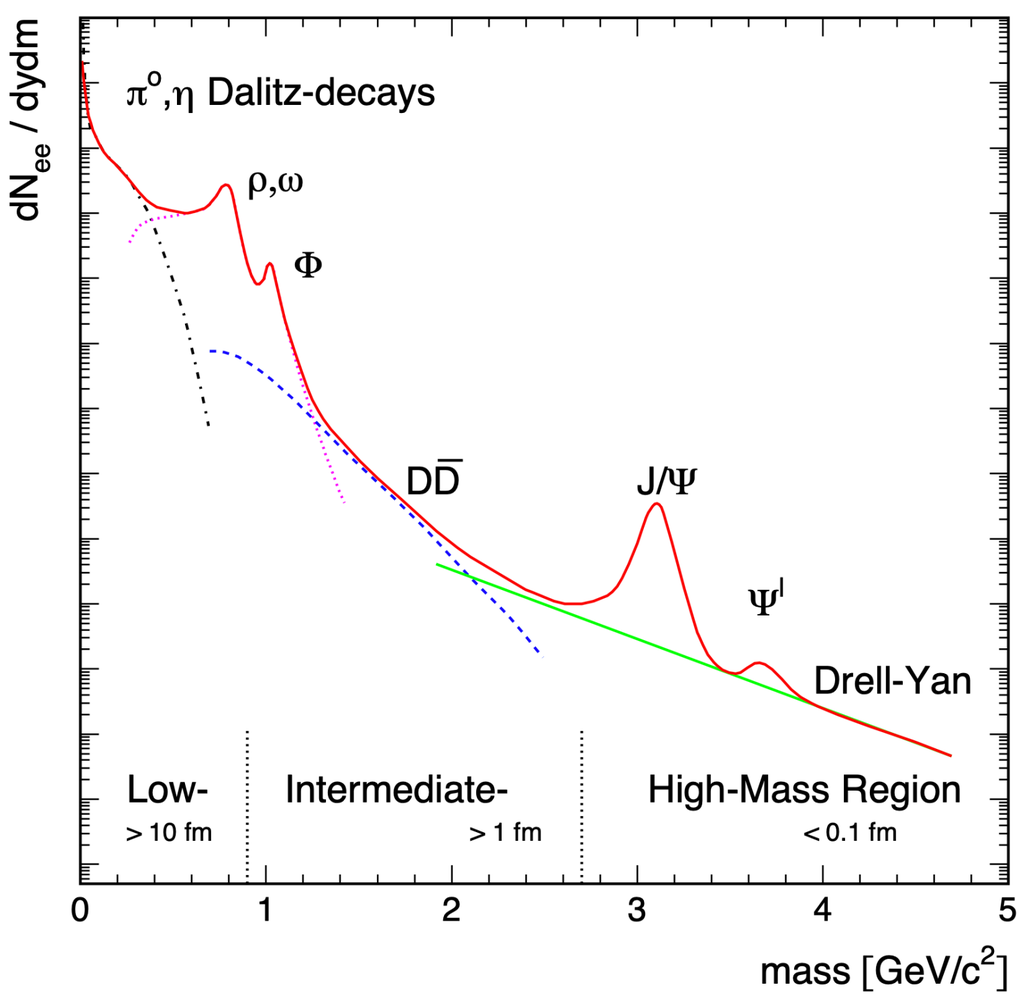

courtesy of Axel Drees

Electromagnetic production rate

In a strongly interacting thermal equilibrium medium Dilepton emission rate in four-dimensional space and momentum

$$\frac{dR_{l^+l^-}}{d^4x\,d^4q} = \frac{-\alpha_{\mathrm{EM}}^2}{3\pi^3 M^2} f_B(q_0;T)\, g_{\mu\nu}\ \mathrm{Im}\left[\Pi_{\mathrm{EM}}^{\mu\nu}(M,q;T,\mu_B)\right]$$

$f_B(q_0;T)$: Thermal Bose–Einstein distribution

$\mathrm{Im}[\Pi_{EM}^{\mu\nu}(M,q;T,\mu_B)]$: Imaginary part of EM correlation function

The emission rate is connected to the imaginary part of correlation function defined via the hadronic EM current

$$\Pi_{\mathrm{EM}}^{\mu\nu}(M,q;T,\mu_B) = -\,i\int d^4x\, e^{iq\cdot x}\,\Theta(x_0)\langle\langle[j_{\mathrm{EM}}^{\mu}(x), j_{\mathrm{EM}}^{\nu}(0)]\rangle\rangle$$

$\Theta(x_0)$: Heaviside function with time (x_0)

E. L. Feinberg, Nuovo Cim. A 34, 391 (1976).
L. D. McLerran and T. Toimela, Phys. Rev. D 31, 545 (1985).

EM spectral function and Vector Meson Dominance

EM spectral function:

- M_{ee} > 1.5 GeV/c^2: Partonic dominance

$$j^{\mu}_{EM} = \sum_{q=u,d,s} e_q \bar{q}\gamma^{\mu} q$$

- M_{ee} < 1.1 GeV/c^2: Vector Meson dominance (VDM)

$$j^{\mu}_{EM} = \frac{1}{2}(\bar{u}\gamma^{\mu}u - \bar{d}\gamma^{\mu}d) + \frac{1}{6}(\bar{u}\gamma^{\mu}u + \bar{d}\gamma^{\mu}d) + \frac{1}{3}\bar{s}\gamma^{\mu}s$$

$$= \frac{1}{\sqrt{2}} j^{\mu}_{\rho} + \frac{1}{3\sqrt{2}} j^{\mu}_{\omega} + \frac{1}{3} j^{\mu}_{\phi}$$

- ρ dominance $\mathrm{Im}\,\Pi_{EM} \sim [\mathrm{Im}\,D_{\rho} + \frac{1}{9}\mathrm{Im}\,D_{\omega} + \frac{2}{9}\mathrm{Im}\,D_{\phi}]$

R.L. Workman et al. (Particle Data Group), Prog. Theor. Exp. Phys. 2022, 083C01 (2022)

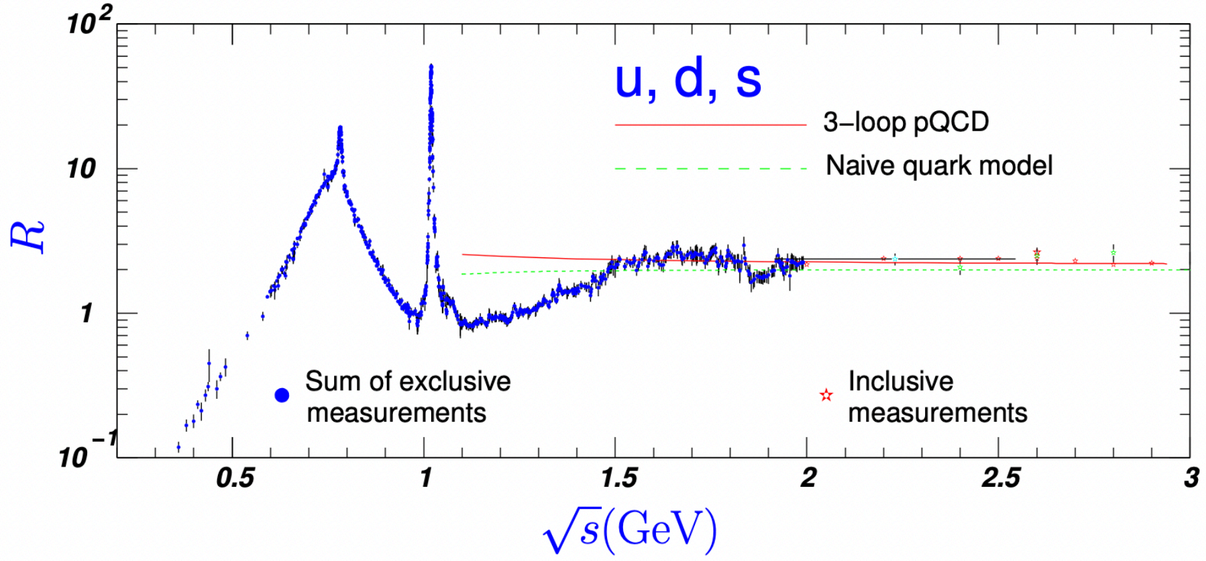

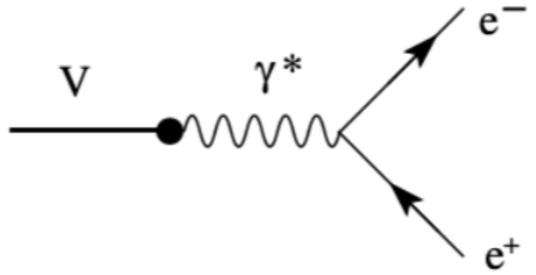

$$R = \frac{\sigma(e^-e^+ \to hadron)}{\sigma(e^-e^+ \to \mu^-\mu^+)}$$

J. J. Sakurai, Currents and Mesons, University of Chicago Press, Chicago (1969).

EM spectral function and Vector Meson Dominance

EM spectral function:

- M_{ee} > 1.5 GeV/c^2: Partonic dominance

$$j^{\mu}_{EM} = \sum_{q=u,d,s} e_q \bar{q}\gamma^{\mu} q$$

- M_{ee} < 1.1 GeV/c^2: Vector Meson dominance (VDM)

$$j^{\mu}_{EM} = \frac{1}{2}(\bar{u}\gamma^{\mu}u - \bar{d}\gamma^{\mu}d) + \frac{1}{6}(\bar{u}\gamma^{\mu}u + \bar{d}\gamma^{\mu}d) + \frac{1}{3}\bar{s}\gamma^{\mu}s$$

$$= \frac{1}{\sqrt{2}} j^{\mu}_{\rho} + \frac{1}{3\sqrt{2}} j^{\mu}_{\omega} + \frac{1}{3} j^{\mu}_{\phi}$$

- ρ dominance $\mathrm{Im}\,\Pi_{EM} \sim [\mathrm{Im}\,D_{\rho} + \frac{1}{9}\mathrm{Im}\,D_{\omega} + \frac{2}{9}\mathrm{Im}\,D_{\phi}]$

J. J. Sakurai, Currents and Mesons, University of Chicago Press, Chicago (1969).

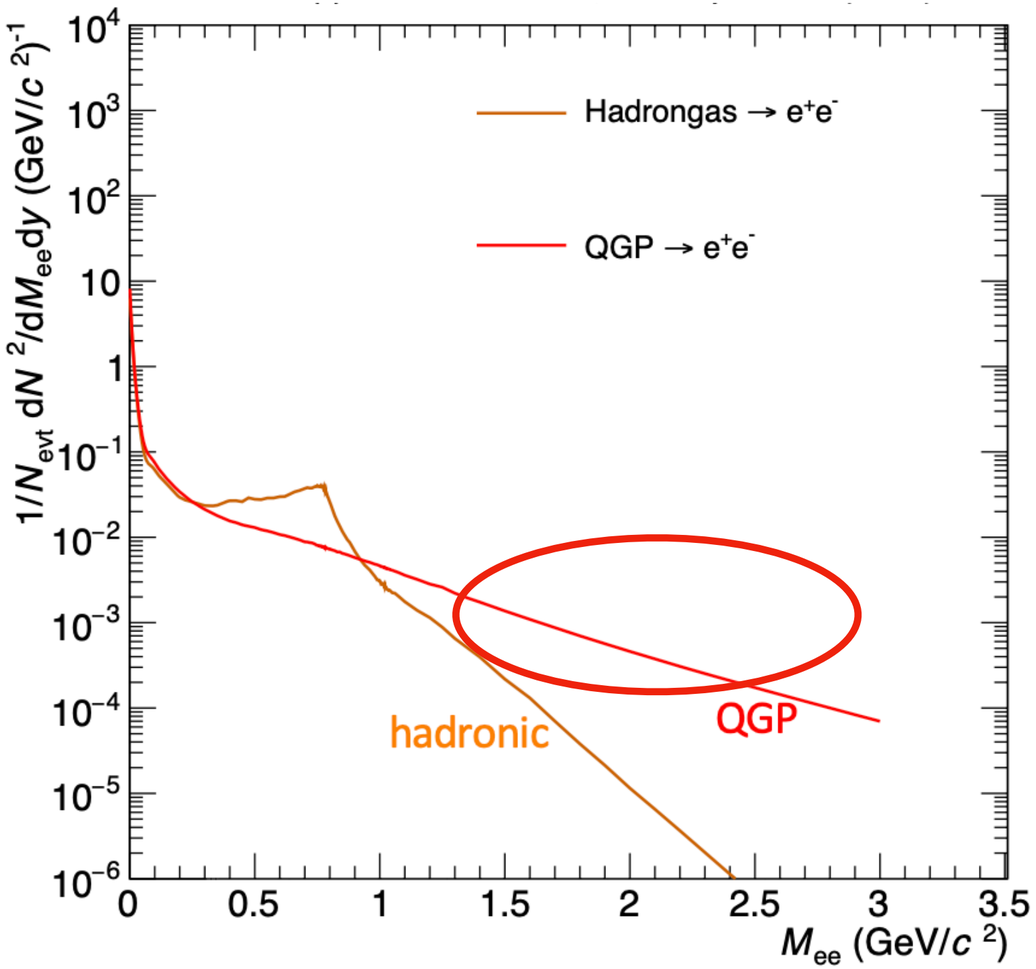

R. Rapp and J. Wambach, Eur. Phys. J. A 6, 415 (1999).

EM spectral function and Vector Meson Dominance

EM spectral function:

- M_{ee} > 1.5 GeV/c^2: Partonic dominance

$$j^{\mu}_{EM} = \sum_{q=u,d,s} e_q \bar{q}\gamma^{\mu} q$$

- M_{ee} < 1.1 GeV/c^2: Vector Meson dominance (VDM)

$$j^{\mu}_{EM} = \frac{1}{2}(\bar{u}\gamma^{\mu}u - \bar{d}\gamma^{\mu}d) + \frac{1}{6}(\bar{u}\gamma^{\mu}u + \bar{d}\gamma^{\mu}d) + \frac{1}{3}\bar{s}\gamma^{\mu}s$$

$$= \frac{1}{\sqrt{2}} j^{\mu}_{\rho} + \frac{1}{3\sqrt{2}} j^{\mu}_{\omega} + \frac{1}{3} j^{\mu}_{\phi}$$

- ρ dominance $\mathrm{Im}\,\Pi_{EM} \sim [\mathrm{Im}\,D_{\rho} + \frac{1}{9}\mathrm{Im}\,D_{\omega} + \frac{2}{9}\mathrm{Im}\,D_{\phi}]$

J. J. Sakurai, Currents and Mesons, University of Chicago Press, Chicago (1969).

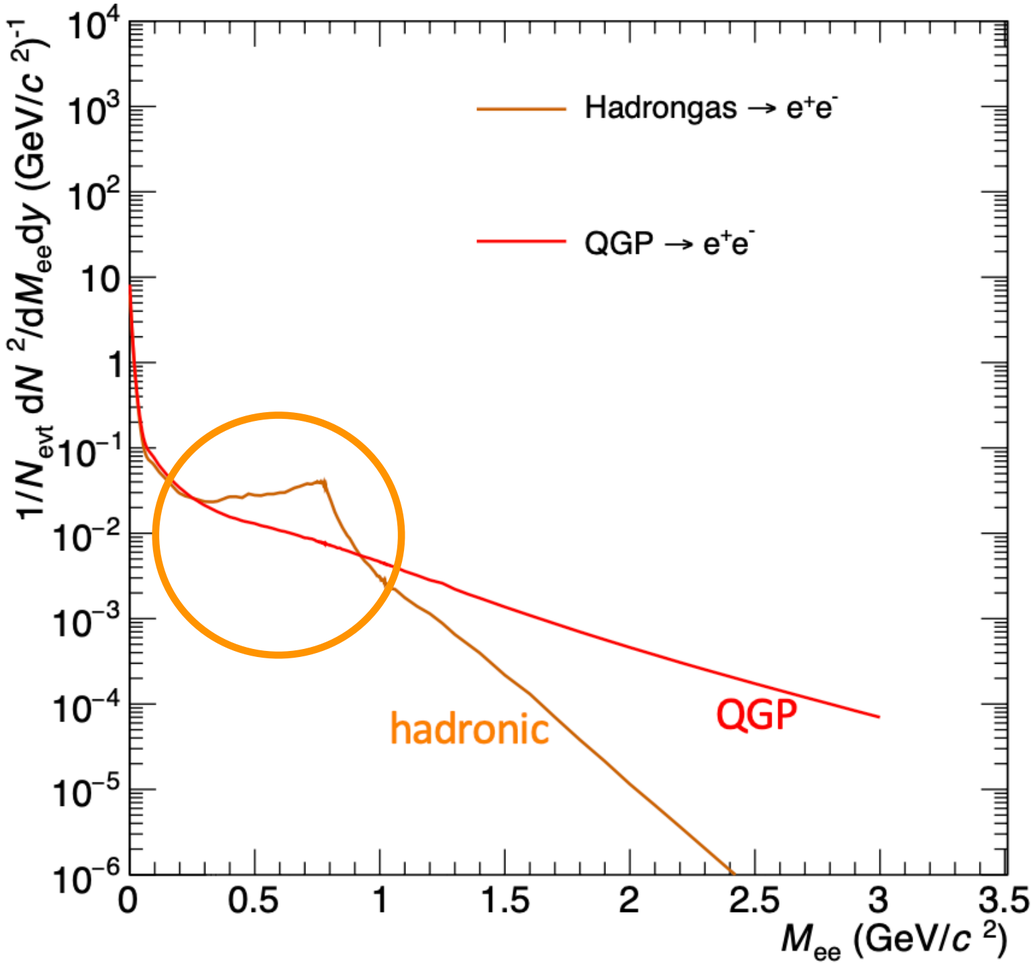

R. Rapp and J. Wambach, Eur. Phys. J. A 6, 415 (1999).

In-medium Hadronic many body approach

ρ meson propagator in the hot and dense hadronic matter

$$D_\rho(q_0, q; \mu_B, T) = \frac{1}{M^2 - (m_\rho^0)^2 - \Sigma_{\rho\pi\pi} - \Sigma_{\rho M} - \Sigma_{\rho B}}$$

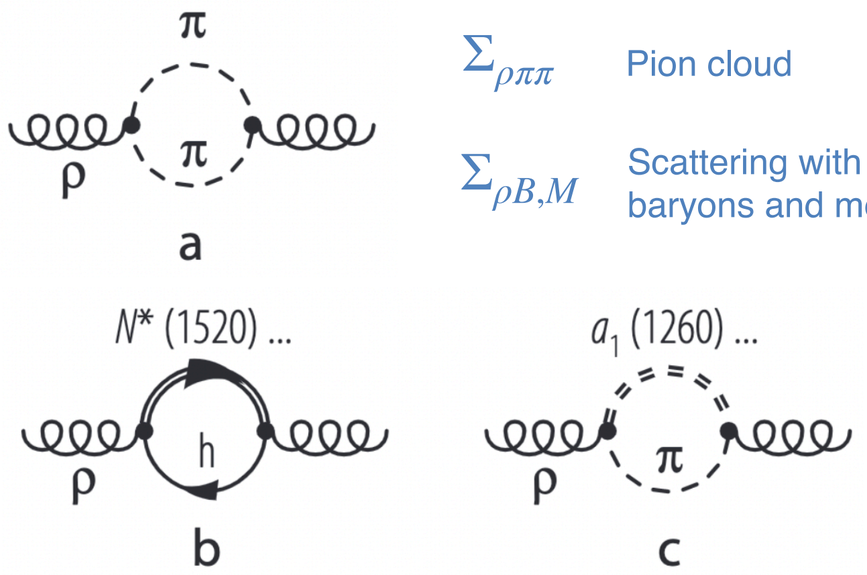

$\Sigma_{\rho\pi\pi}$ Pion cloud

$\Sigma_{\rho B,M}$ Scattering with baryons and mesons

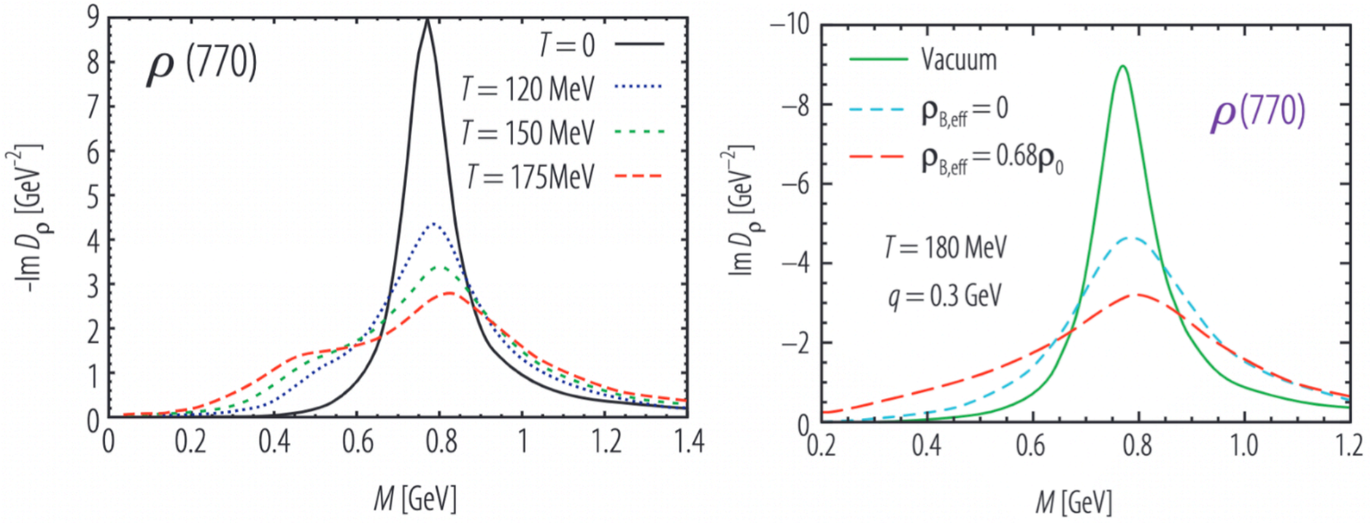

Width broadening depends on Temperature and Baryon Density

R. Rapp and C. Gale, Phys. Rev. C 60, 024903 (1999).
R. Rapp, G. Chanfray, and J. Wambach, Nucl. Phys. A 617, 472-495 (1997).
M. Herrman, B. L. Friman and W. Nörenberg, Nucl. Phys. A 560, 411 (1993).

R. Rapp and J. Wambach, Eur. Phys. J. A 6, 415 (1999).
M. Urban, M. Buballa, R. Rapp, and J. Wambach, Nucl. Phys. A 673, 357 (2000).
Rapp, Acta Phys. Polon. B42 (2011) 2823.

In-medium ρ meson spectral function study

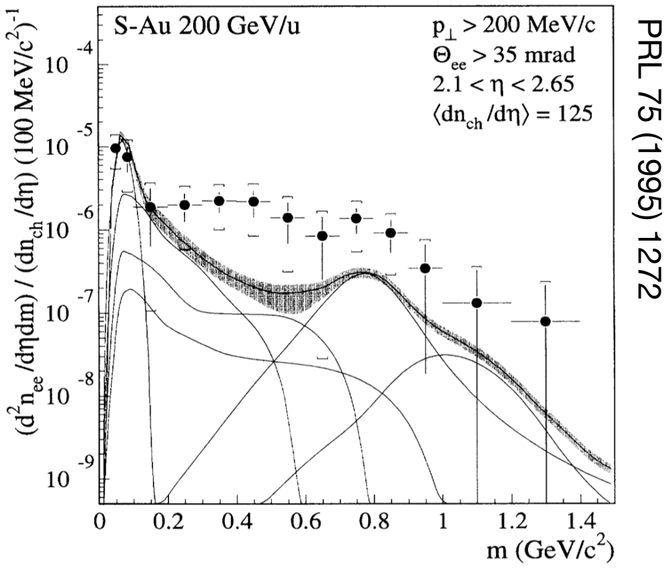

PRL 75 (1995) 1272

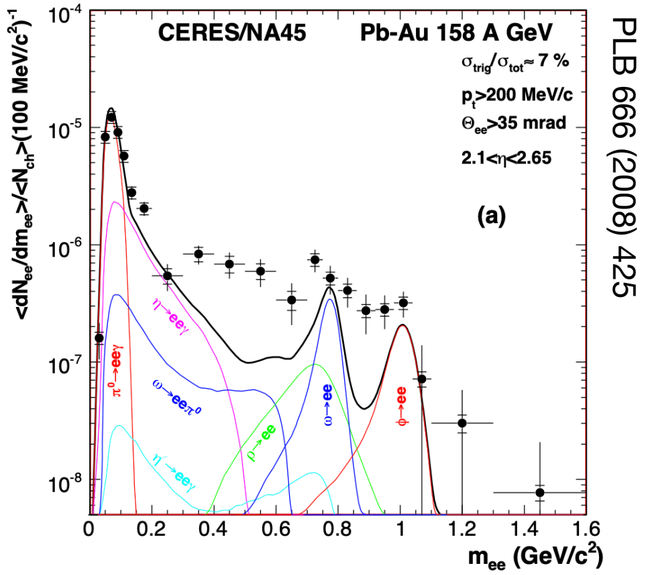

PLB 666 (2008) 425

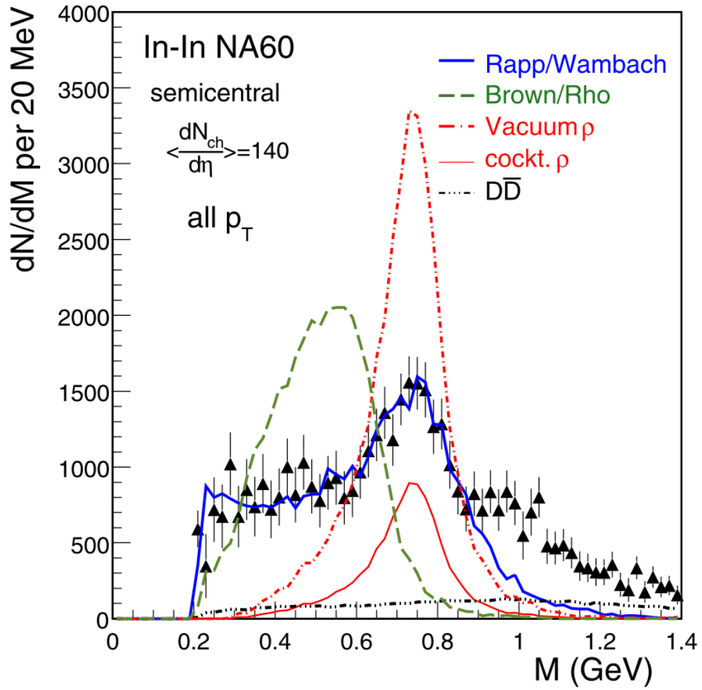

EPJ C61 (2009) 711

- Vacuum ρ can't describe strong enhancement.
- Dropping mass scenario (Brown-Rho)?
- Broadening of ρ spectral function (Rapp-Wambach).

Rules out dropping mass scenario.
Agreement with width broadening in LMR.

Dileptons as thermometer at NA60

- Thermal dielectrons can directly access the hot QCD medium at both QGP phase and hadronic phase.

- NA60: IMR dilepton rate in non-relativistic approximation:

$$\frac{dR_{ll}}{dM} \propto (MT)^{\frac{3}{2}} e^{-M/T} \longrightarrow \langle T \rangle = 205 \pm 12 MeV$$

range $1.2 < M_{ll} < 2.0$ GeV/c²

- Independent of flow: no blue shift effects.
- Exceeding the pseudo-critical temperature computed in thermal lattice-QCD.

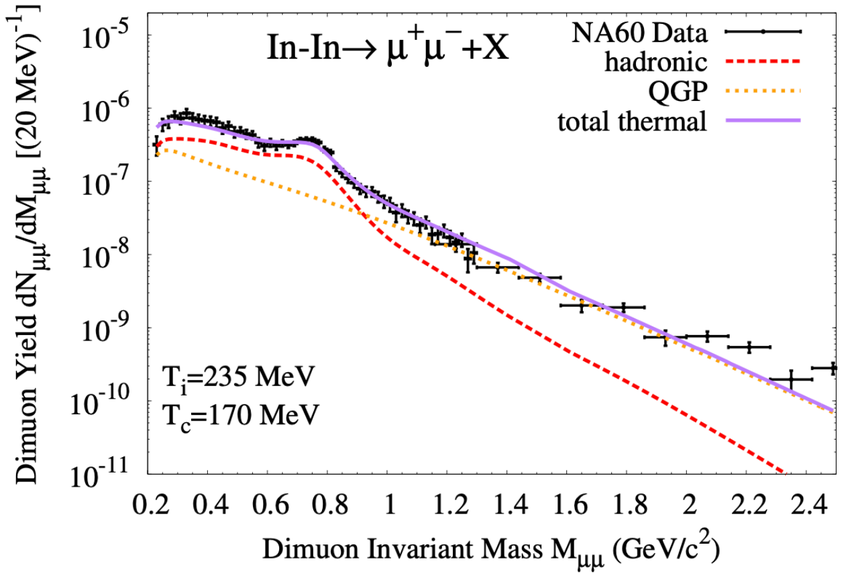

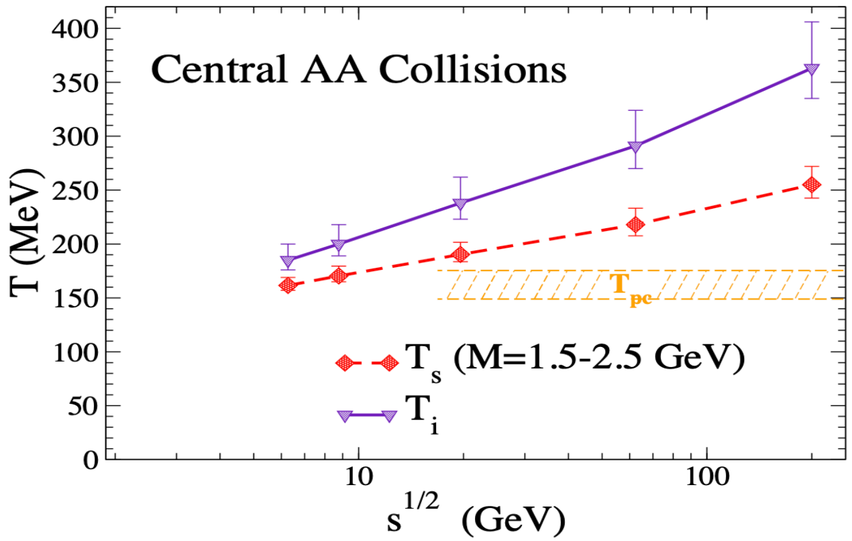

R. Arnaldi et al. (NA60), EPJC 61(2009) 711
NA60, AIP Conf.Proc. 1322 (2010) 1
Rapp, van Hees, PLB 753 (2016) 586

Relativistic Heavy-Ion Collider

- Electron beam ion source (EBIS):
  - Generate Ion Beam 2 MeV/nucleon.
- Linear Accelerator (LINAC): proton source.
- Booster Synchrotron:
  - Accelerates ions to 100 MeV/nucleon, Q = +77.
- Alternating Gradient Synchrotron (AGS):
  - Accelerates ions to 8.86 GeV/nucleon, Q = +79.
  - Convey ion beam into RHIC.

- Relativistic Heavy-Ion Collider(RHIC):
  - The Solenoidal Tracker At RHIC (STAR) — Detector for this thesis.
  - sPHENIX experiment.
  - Two hexagonal storage ring.
    - Blue (clockwise) and Yellow (counter-clockwise).

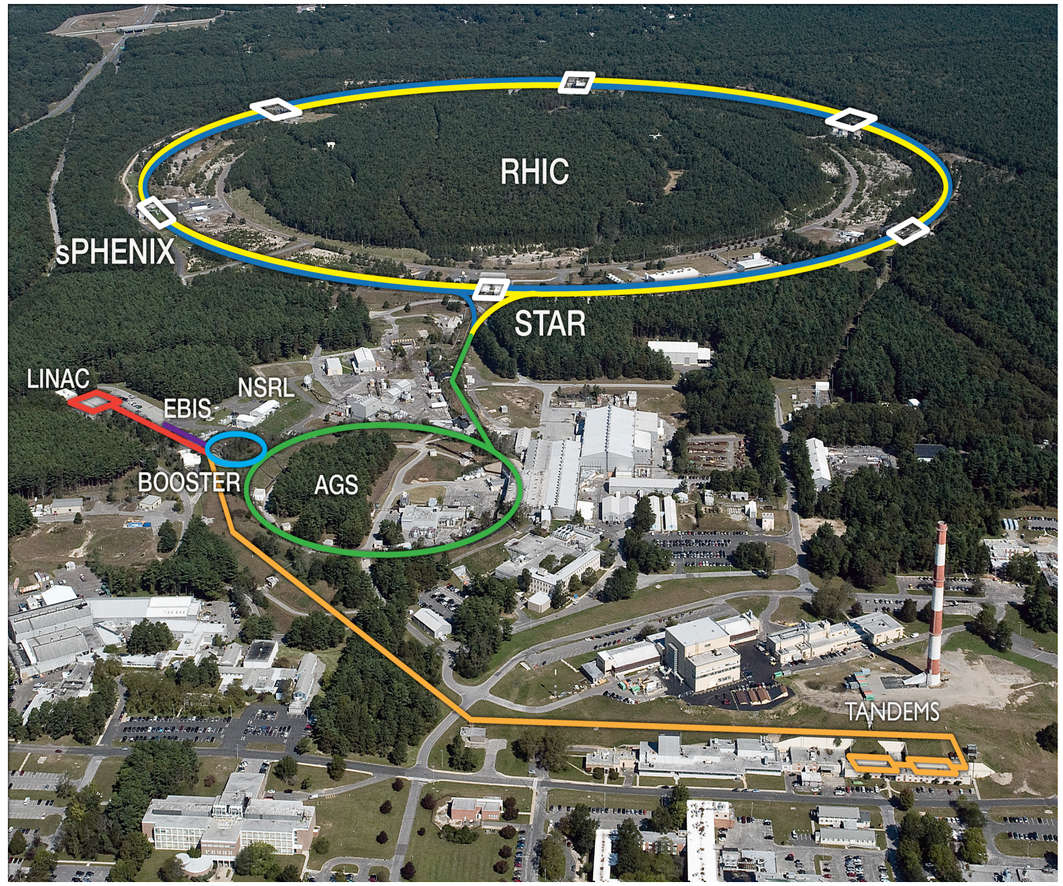

The Solenoidal Tracker At RHIC (STAR)

STAR Beam Use Request 2019/2020 (SN696)
STAR, Nature Physics 16, 409-412 (2020)

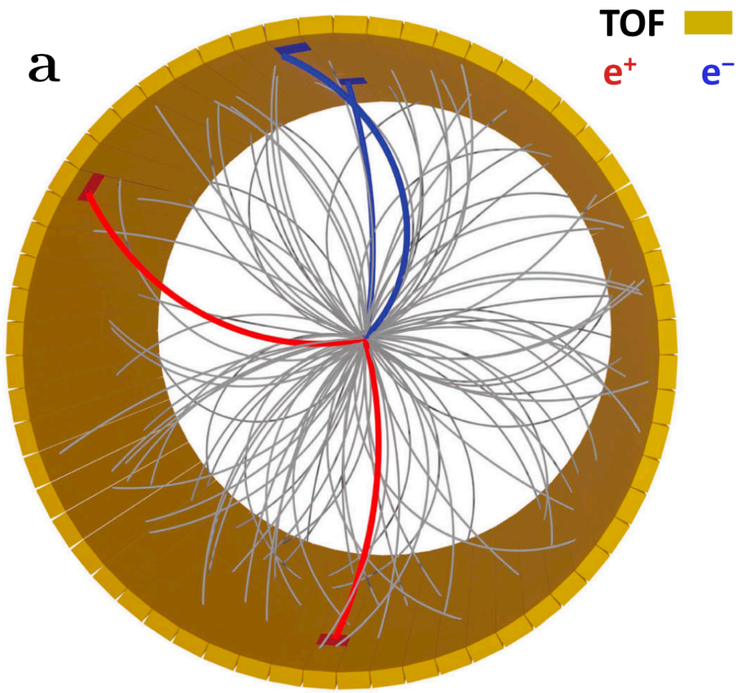

- Time Projection Chamber (TPC).
- 0.5 T solenoidal magnet.
- Time of Flight Detector (TOF).

STAR Trigger System

- STAR minimum-bias (MB) trigger criteria:
  - A coincidence of signals in both the -z and +z detector components: BBC || VPD || ZDC.
- Beam-Beam Counter (BBC):
  - Located |z| = 3.75 m from STAR detector center.
  - Detect charged particles.
- Vertex Position Detector (VPD):
  - Located |z| = 5.6 m from STAR detector center.
  - Detect photons.
- Zero Degree Calorimeter (ZDC):
  - Located |z| = 18 m from STAR detector center.
  - Detect neutrons.

STAR electron identification method: TPC + TOF

b

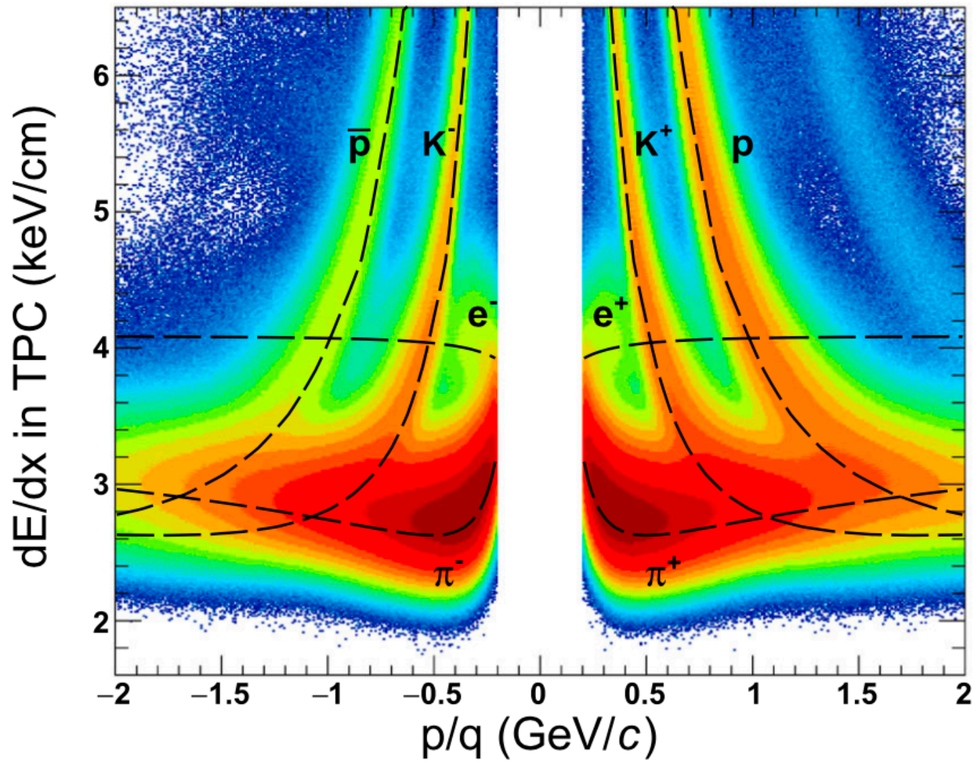

c

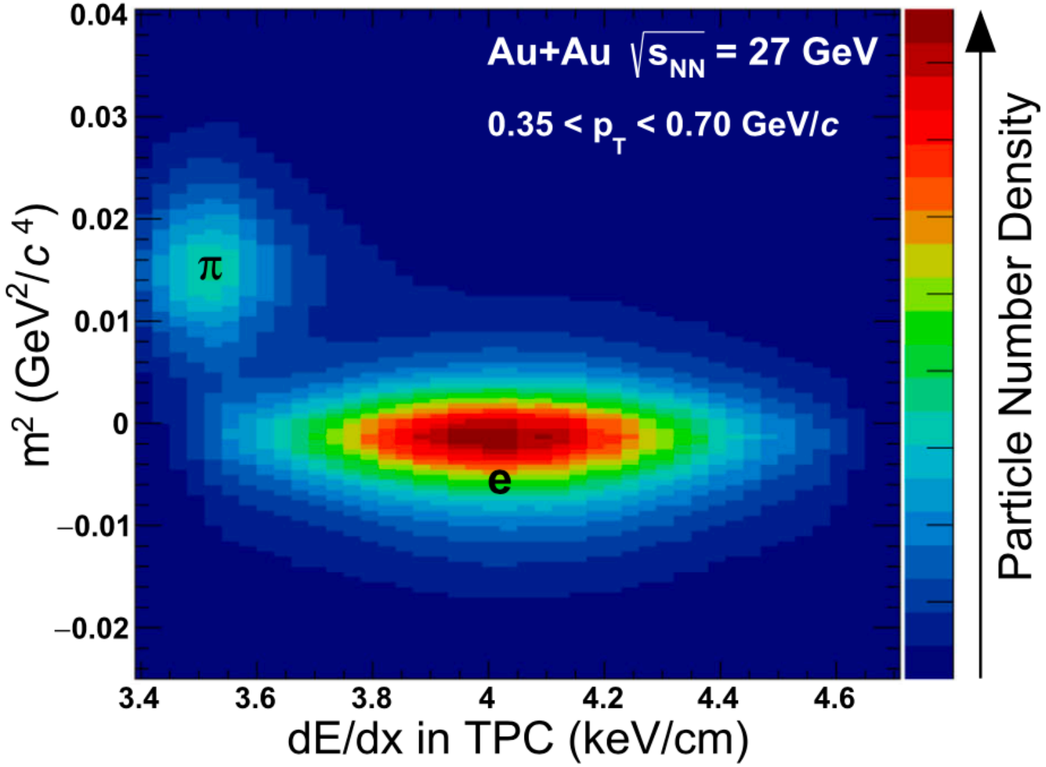

BES-I dielectron production

- Explore low-mass range down to SPS energies.
- Excess yield is well described by the in-medium ρ + QGP emission models.
- Normalized excess yield shows no significant $\sqrt{s_{NN}}$ dependence.
- Limited precision especially at low collision energies.

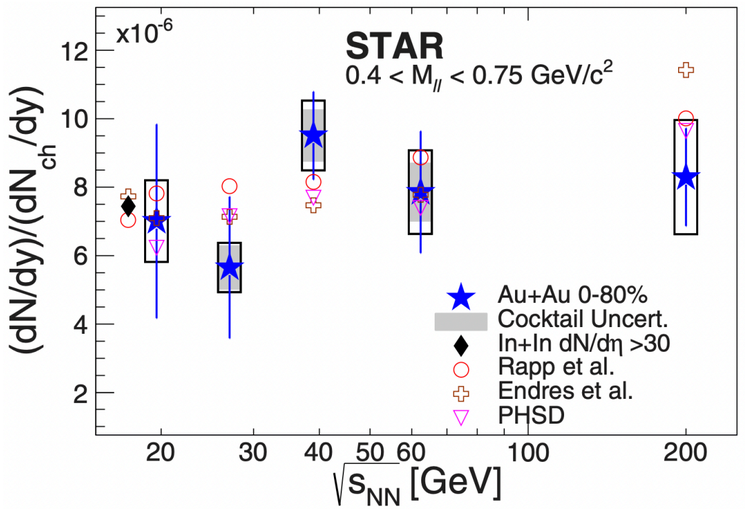

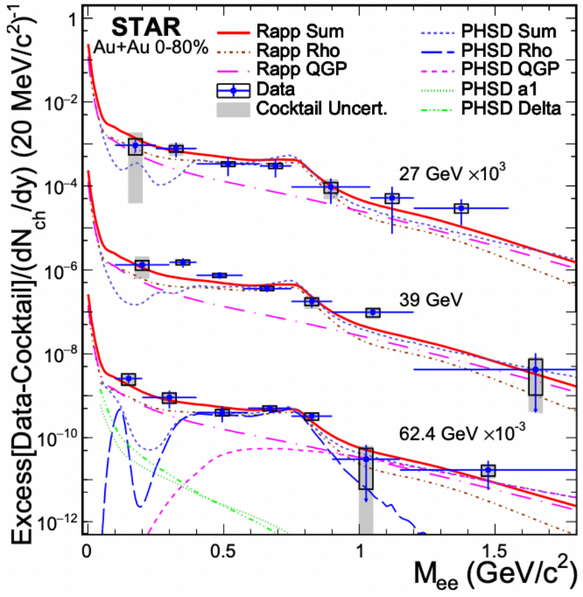

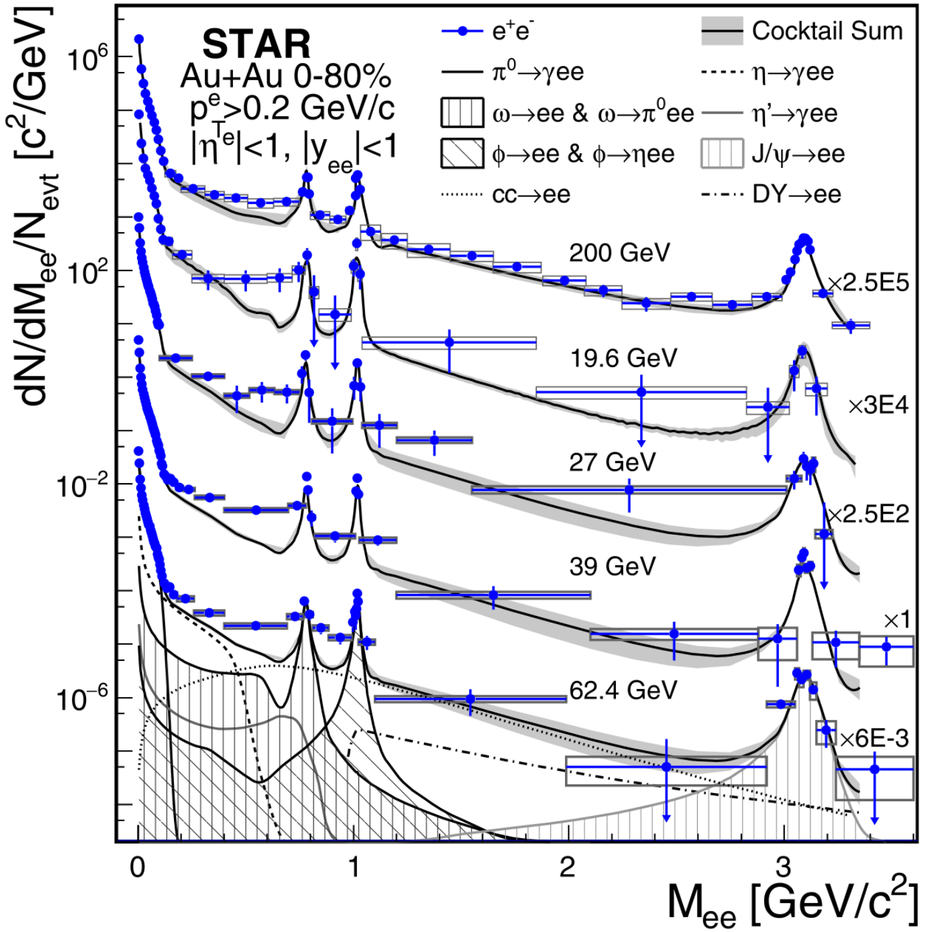

STAR: Phys. Rev. C 107, L061901 (2023)
STAR: Phys. Lett. B 750, (2015) 64
STAR: Phys. Rev. C 92, 024912 (2015)

From BES-I to BES-II

- BES-I dielectron results ($\sqrt{s_{NN}}$: 19.6 - 200 GeV):
  - Kinetic/chemical freeze-out temperatures and total baryon densities are approximately constant.
  - Variations in fireball lifetime appear to have minimal impact on the normalized yield.

STAR: Phys. Rev. C 96, 044904 (2017)

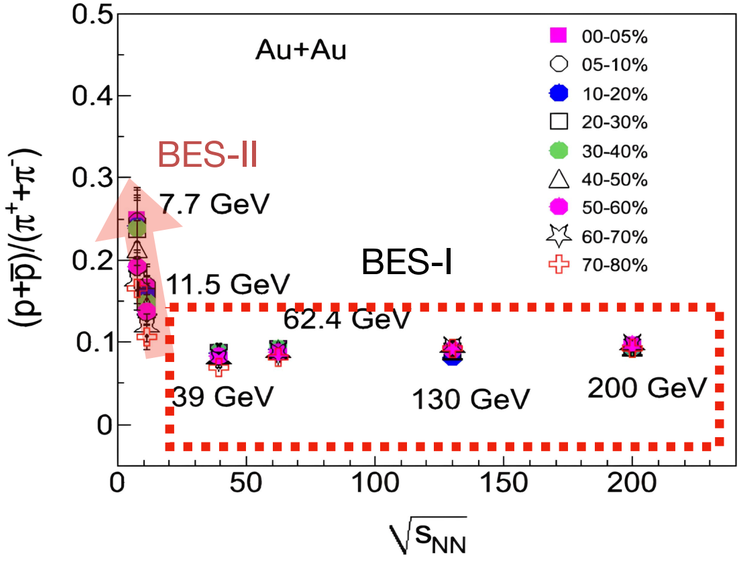

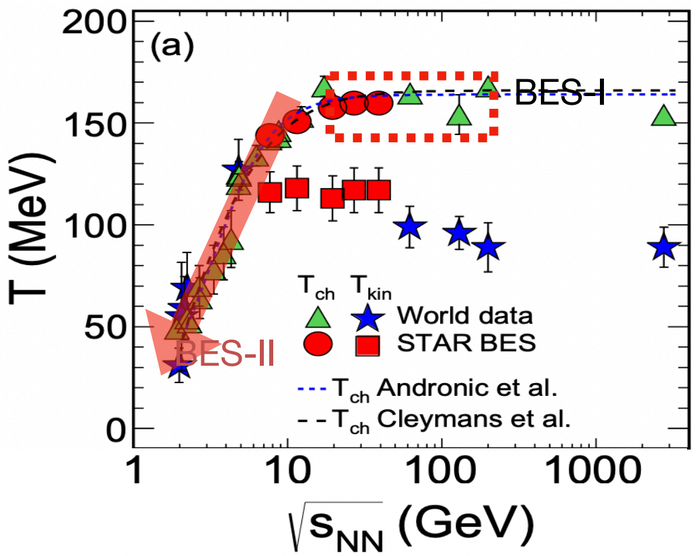

- BES-II study enters high-μ_B regime ($\sqrt{s_{NN}}$ between 7.7 and 19.6 GeV).
  - The total baryon density increases rapidly, while the temperature exhibits only a slight decrease. Probe **baryon-density effects** on the EM excitation function.
  - Total baryon density and temperature have opposite effect on the results. Systematic measurements across beam energies help disentangle competing effects.

BES-II dielectron production

- Efficiency-corrected dielectron invariant mass spectra within the STAR acceptance for Au+Au collisions at $\sqrt{S_{NN}}$ = 7.7, 9.2, 11.5, 14.6 and 19.6 GeV.

- ω and φ mesons are clearly visible and are well-described by the hadronic cocktail.

- In the low-mass region (LMR), pronounced excess of dielectrons predominantly from ρ meson decays with thermal radiation from the QGP and hadronic gas.

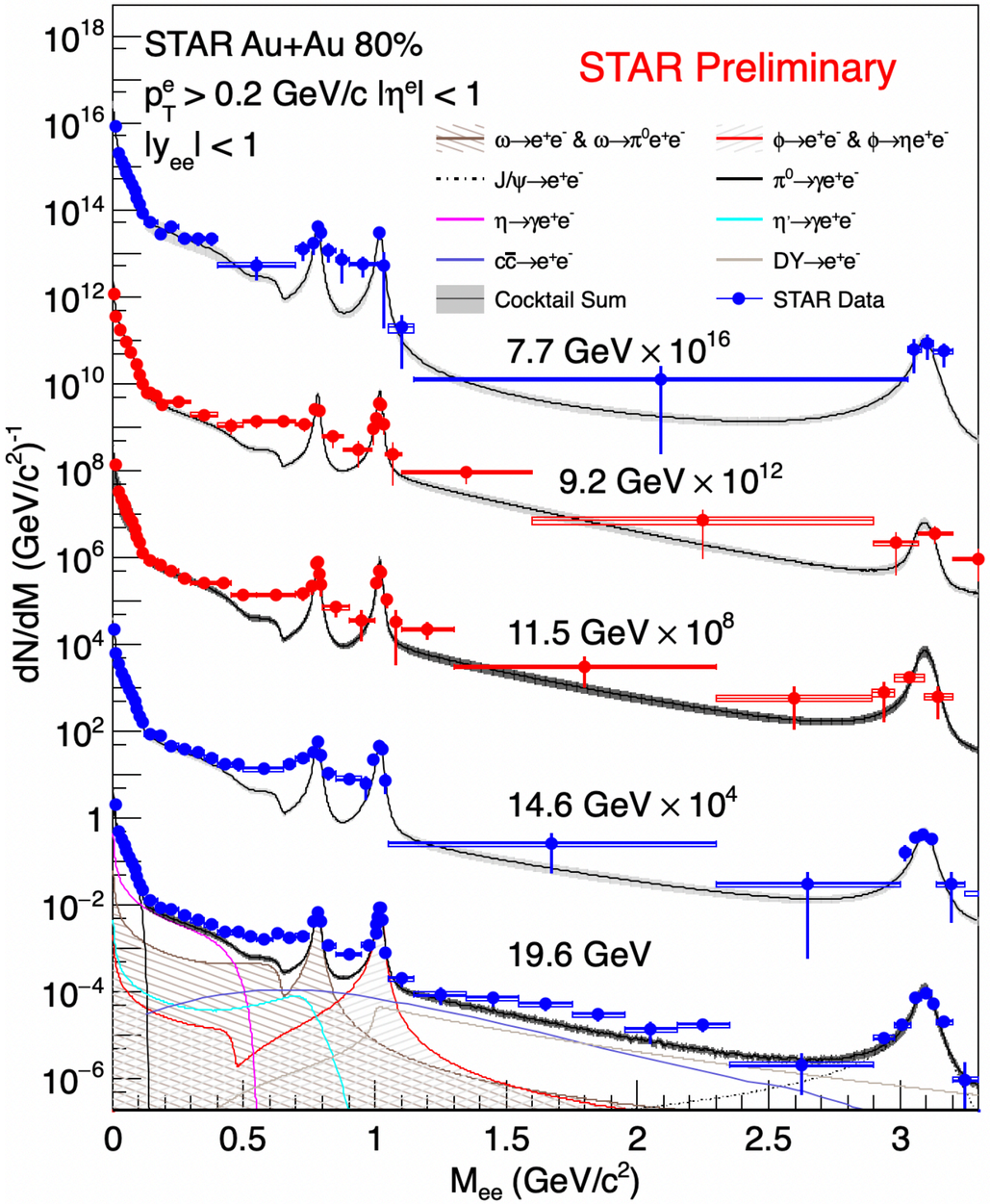

Acceptance Corrected Excess yield

- Acceptance-corrected excess yield invariant mass spectra (points) for Au+Au collisions at $\sqrt{S_{NN}}$ = 7.7, 9.2, 11.5, 14.6 and 19.6 GeV.

- Good agreement with the Vector Meson Dominance (VMD) approach.

- The data support that the ρ resonance "melts" into a continuum of e^+e^- pairs where the ρ meson propagator is modified in the medium.

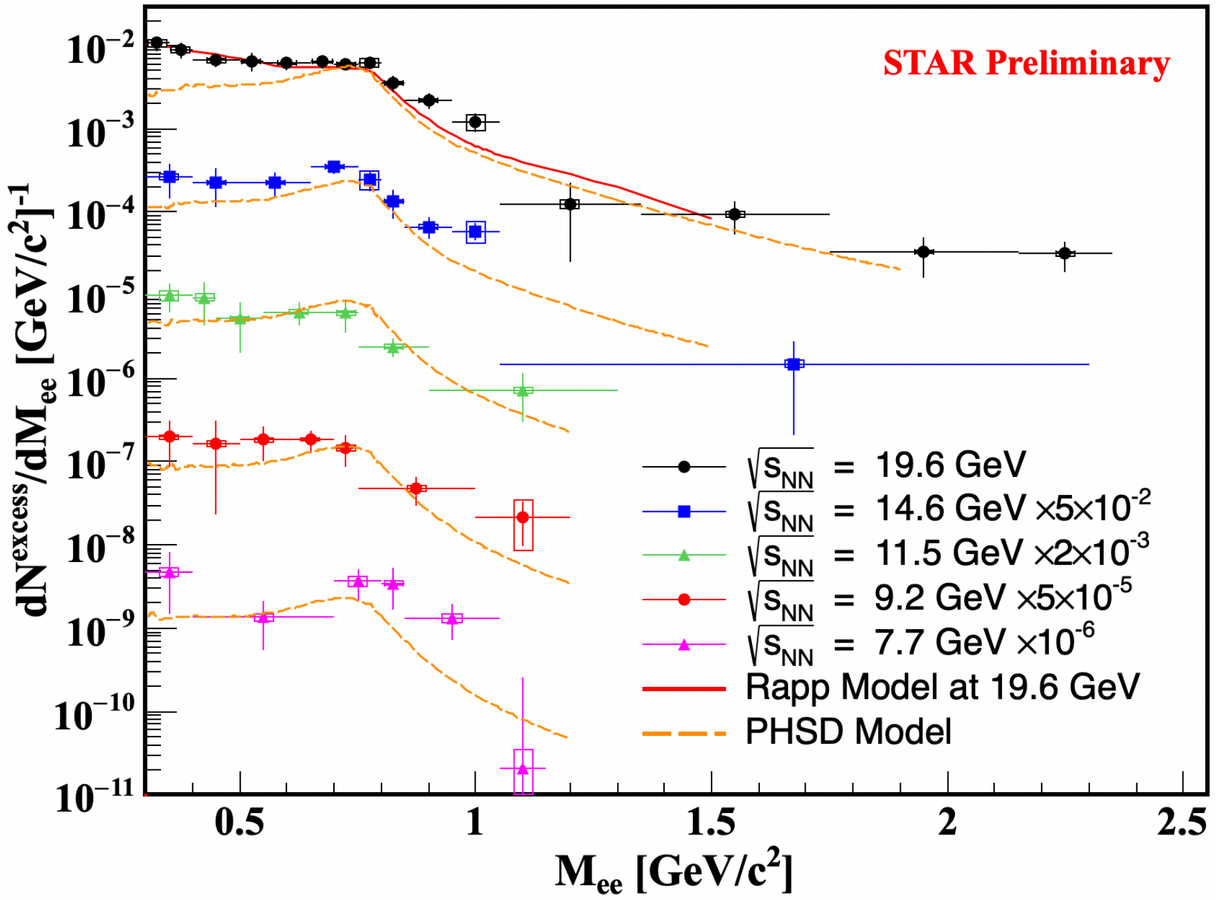

R. Rapp: Phys. Rev. C 63 (2001) 054907, Phys. Rev. Lett. 97, 102301 (2006) ;

Integral of normalized excess yield

- Pion yield normalized integrated excess yield vs. collision energy for $0.4 < M_{ll} < 0.75$ GeV/c^2.

- Data agrees there is a **decreasing trend** in normalized integrated excess yield for Au+Au collisions as the collision energies decreases.

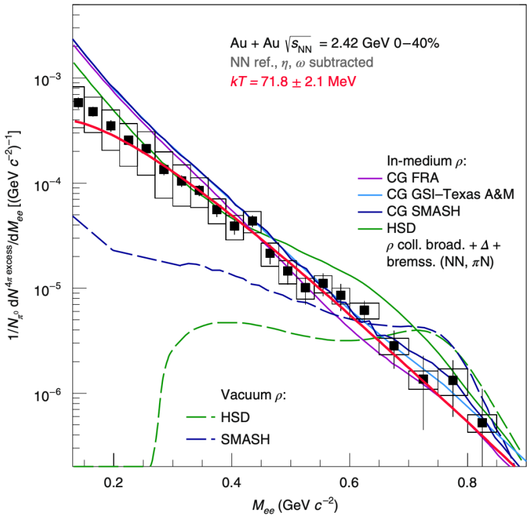

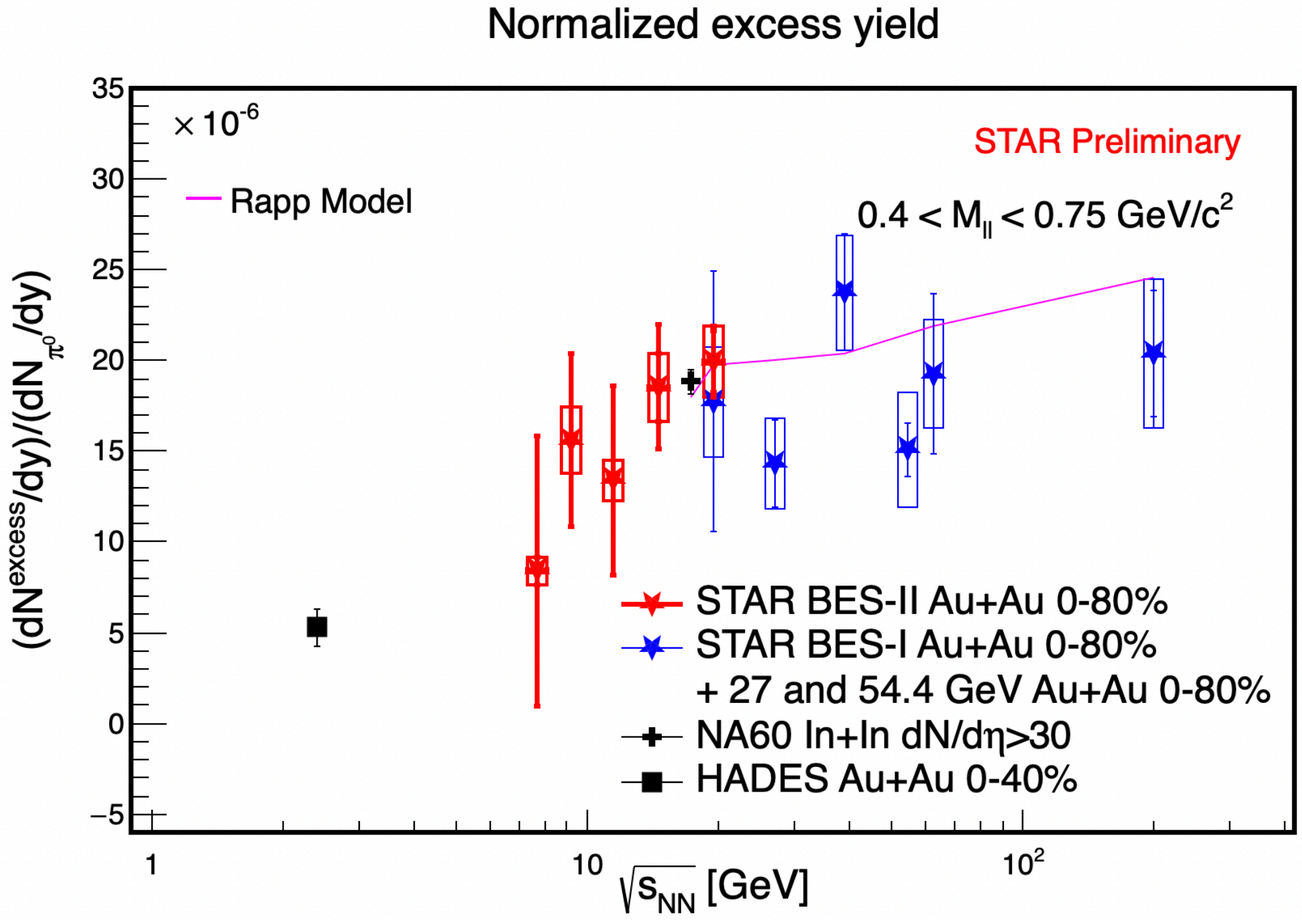

STAR: Nat. Commun. 16, 9098 (2025)
HADES: Nature Physics 15 (2019) 1040
NA60: EPJ C 59 (2009) 607
H. van Hees and R. Rapp, Phys. Rev. Lett. 97, 102301 (2006)

Integral of normalized excess yield compared with PHSD

- The downward trend is contrary to initial PHSD calculations that normalized integrated excess yield will increase with higher total baryon density without temperature effect.

- PHSD: Parton Hadron String Dynamic is a relativistic transport model.

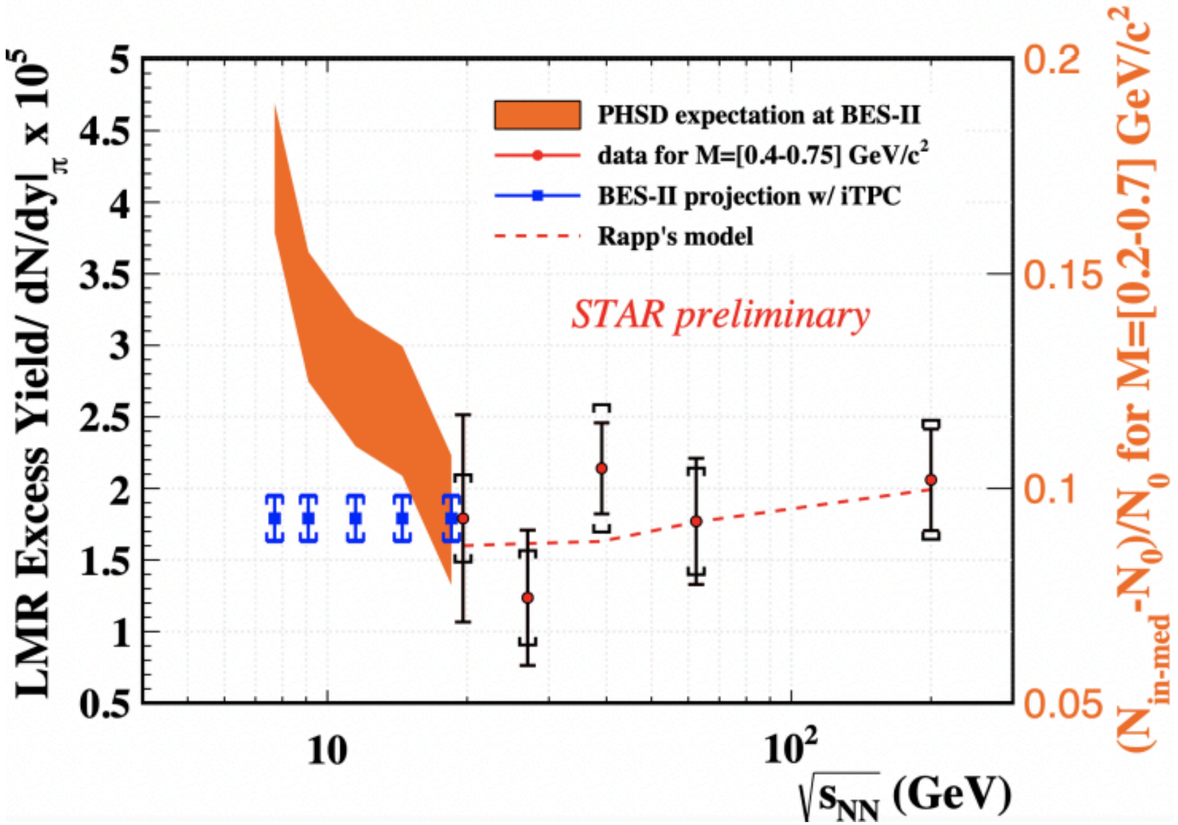

STAR Note SN0598 (2014)

Integral of normalized excess yield compared with PHSD

- **Temperature effects:**
  - At lower collision energies, the fireball temperature decreases, suppressing thermal dilepton production rate. $\Sigma_{\rho M}$
  - Meson-induced scattering decreases as pion density drops.

- **Baryon density effects:**
  - As the collision energy decreases, the baryon density rises sharply. ρ width broadening from the increased interaction cross section between the ρ meson and baryons in the medium $\Sigma_{\rho B}$

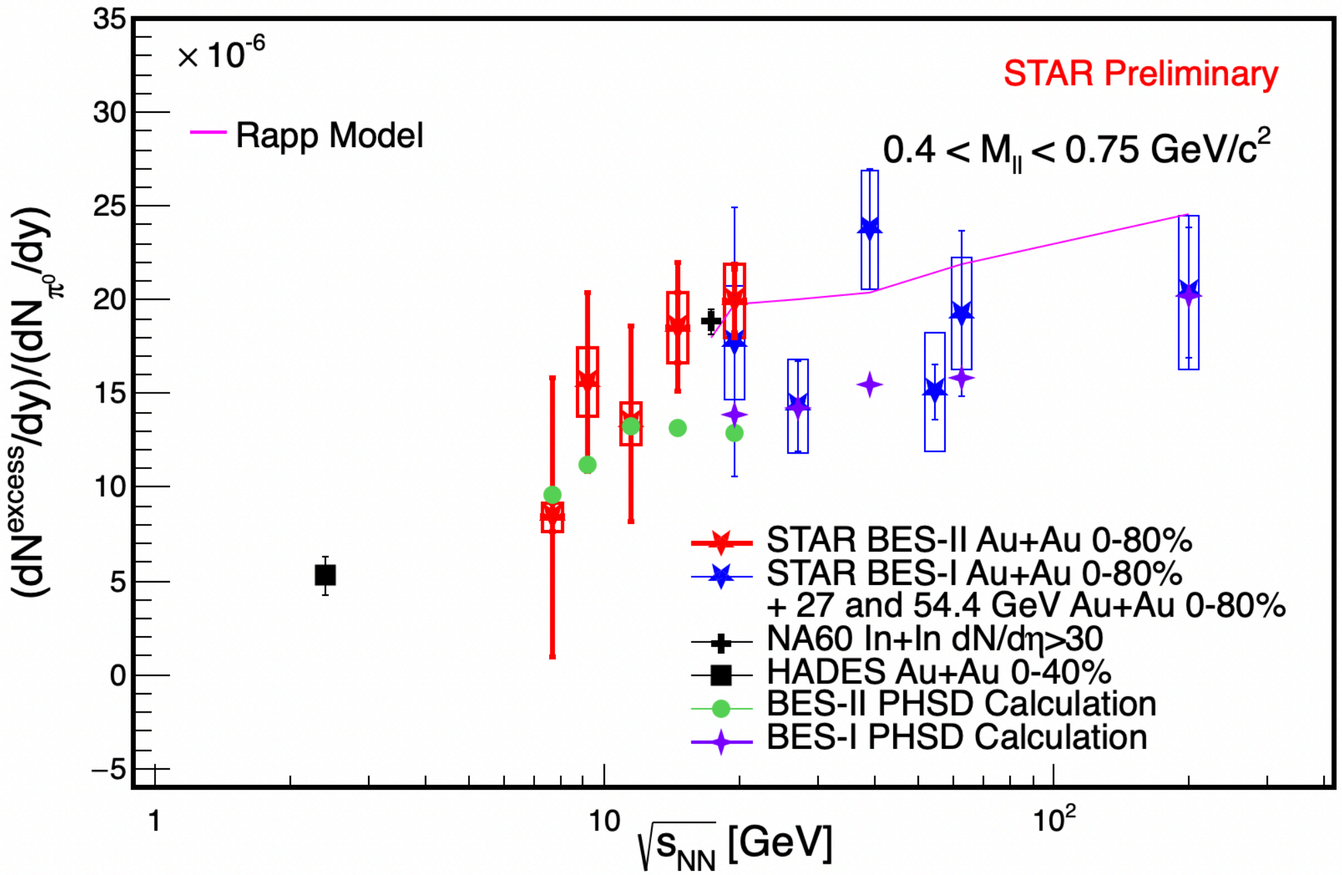

STAR: Nat. Commun. 16, 9098 (2025)
HADES: Nature Physics 15 (2019) 1040
NA60: EPJ C 59 (2009) 607
H. van Hees and R. Rapp, Phys. Rev. Lett. 97, 102301 (2006)
PHSD: Phys. Rev. C 111, 064904 (2025)

Integral of normalized excess yield compared with PHSD

- To reproduce the measured trend, models must incorporate the interplay between baryon chemical potential and the evolving temperature.
  - Updated PHSD calculations successfully reproduce the observed decreasing trend.

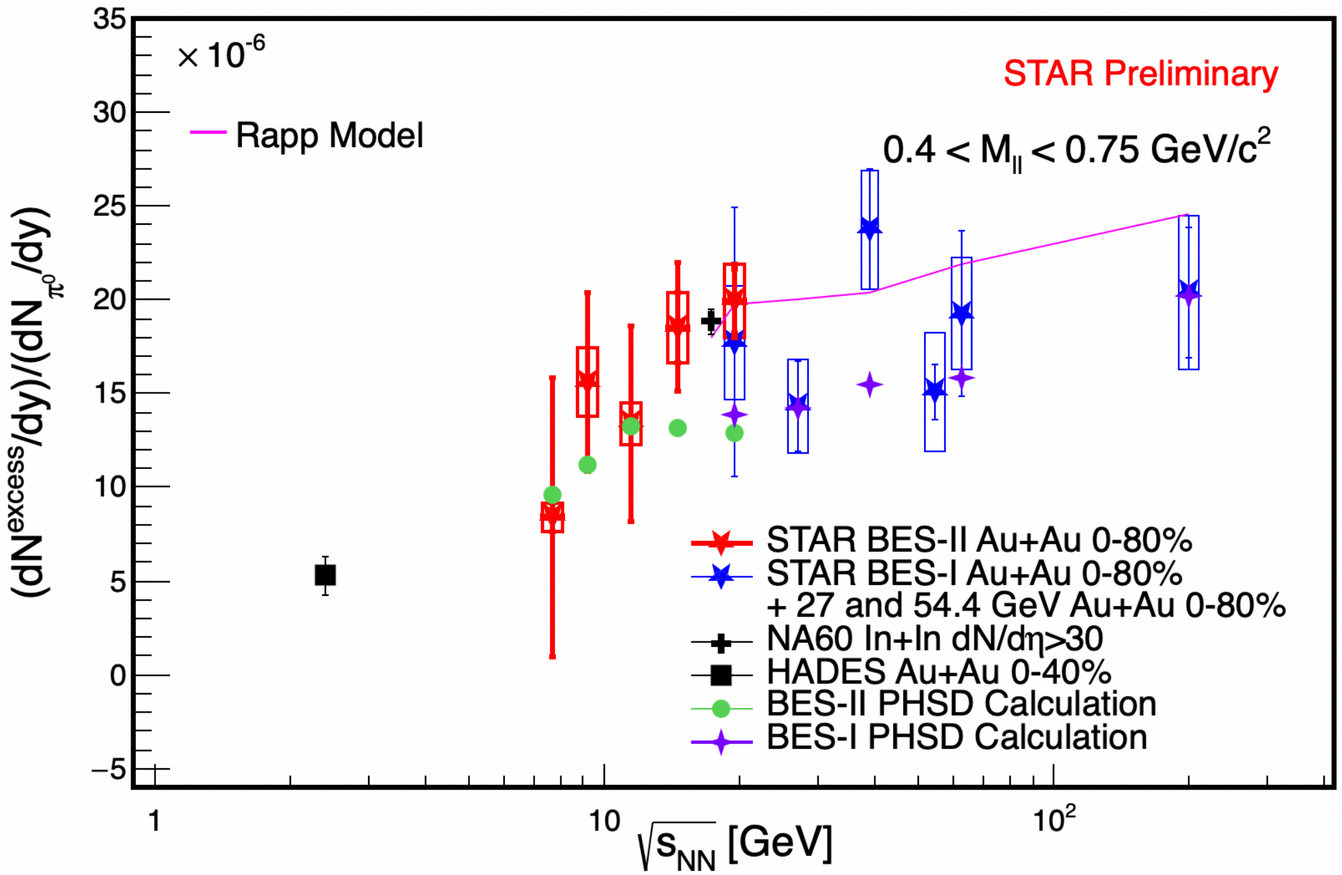

STAR: Nat. Commun. 16, 9098 (2025)
HADES: Nature Physics 15 (2019) 1040
NA60: EPJ C 59 (2009) 607
H. van Hees and R. Rapp, Phys. Rev. Lett. 97, 102301 (2006)
PHSD: Phys. Rev. C 111, 064904 (2025)

Dielectron as thermometer

- Dielectron temperature measurement at $\sqrt{s_{NN}}$ = 27 and 54.4 GeV with STAR experiment.
- QGP radiation: $M^{3/2} * e^{-M/T}$.
- In-medium ρ: Breit-Wigner * $e^{-M/T}$.

Low Mass Range fitting function:

$$(a * f^{BW}(M) + b * M^{3/2}) * e^{-M/T}$$

Breit-Wigner(BW) function:

$$f_{\mathrm{BW}}(M) = \frac{M M_0 \Gamma_{ll}}{\left(M_0^2 - M^2\right)^2 + M_0^2 \Gamma^2}$$

$$\Gamma = \Gamma_0 \frac{M_0}{M} \left(\frac{M^2 - 4m_\pi^2}{M_0^2 - 4m_\pi^2}\right)^{3/2} \quad \Gamma_{ll} \propto \left(1 + \frac{2m_l^2}{M^2}\right)\left(1 - \frac{4m_l^2}{M^2}\right)^{1/2}$$

M: dilepton invariant mass. M_0: rho meson pole mass. Γ_0: rho meson vacuum width

STAR: Nature Communication 16, 9098 (2025)
Rapp, van Hees, PLB 753 (2016) 586
T_{PC}: HotQCD, Phys.Lett.B 795 (2019) 15-21;
NA60: EPJC (2009) 59 607-623

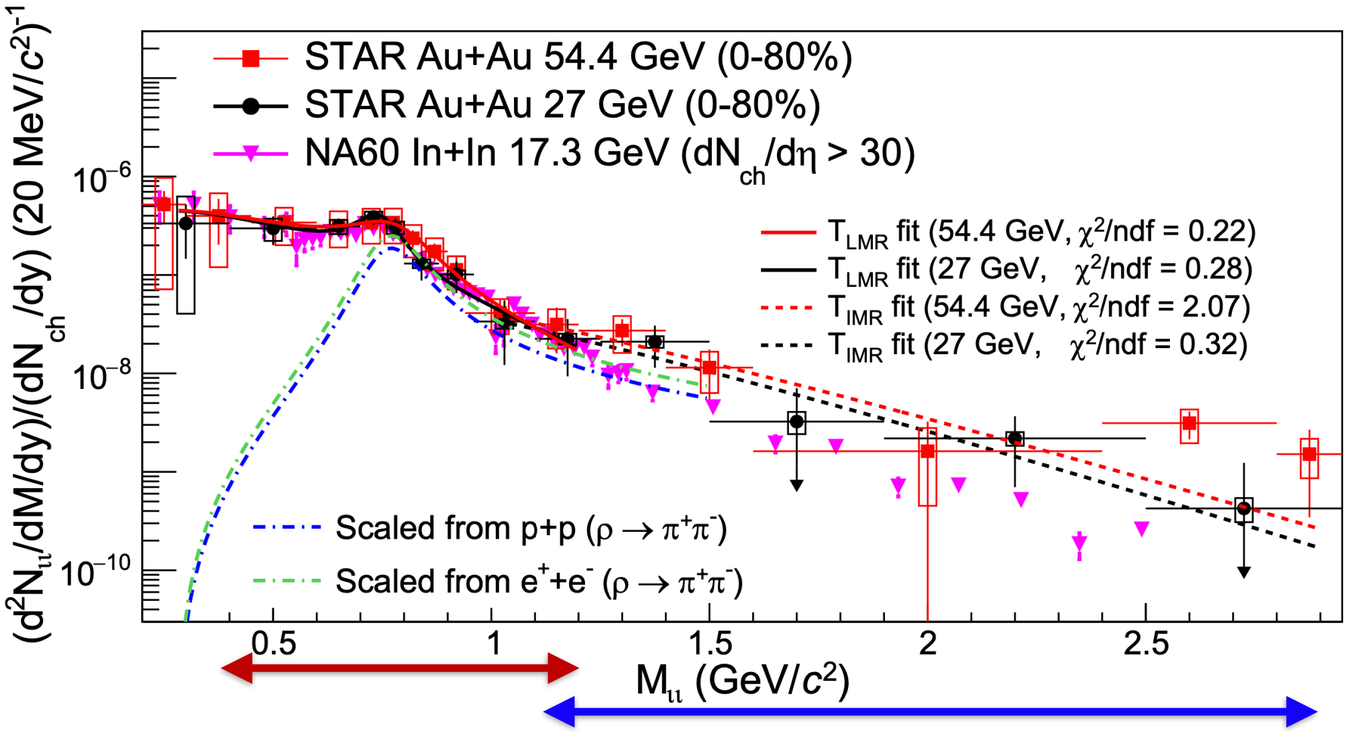

$T_{\mathrm{LMR}}^{54.4\ \mathrm{GeV}} = 178 \pm 15\ (\mathrm{stat.}) \pm 13\ (\mathrm{sys.})\ \mathrm{MeV}$ $T_{\mathrm{IMR}}^{54.4\ \mathrm{GeV}} = 287 \pm 70\ (\mathrm{stat.}) \pm 34\ (\mathrm{sys.})\ \mathrm{MeV}$

$T_{\mathrm{LMR}}^{27\ \mathrm{GeV}} = 165 \pm 20\ (\mathrm{stat.}) \pm 21\ (\mathrm{sys.})\ \mathrm{MeV}$ $T_{\mathrm{IMR}}^{27\ \mathrm{GeV}} = 274 \pm 65\ (\mathrm{stat.}) \pm 10\ (\mathrm{sys.})\ \mathrm{MeV}$

BES-II temperature measurement

- First temperature measurement in STAR BES-II energies.

- 19.6 and 14.6GeV LMR Temperature:
  - T is close to pseudo critical temperature.
  - Results indicate the thermal radiation from hadronic gas is mainly produced around the phase transition.

$$T_{LMR}^{19.6GeV}(0-80\%) = 168 \pm 13(stat.) \pm 15(sys.)\ MeV$$

$$T_{LMR}^{14.6GeV}(0-80\%) = 183 \pm 25(stat.) \pm 21(sys.)\ MeV$$

Low Mass Range fitting function:

$$(a * BW + b * M^{3/2}) * e^{-M/T}$$

Breit-Wigner(BW) function:

$$\frac{M M_0 \Gamma}{(M_0^2 - M^2)^2 + M_0^2 \Gamma^2}$$

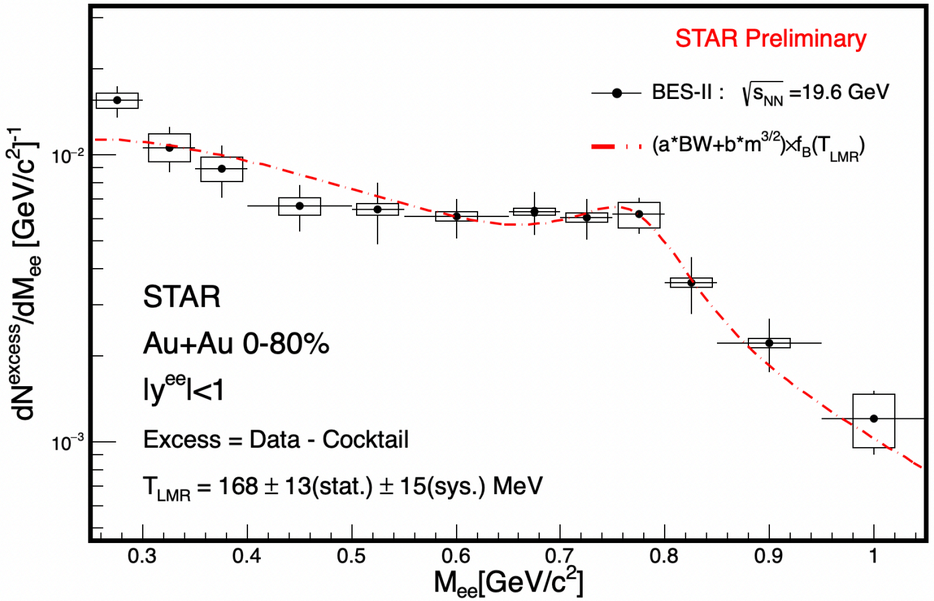

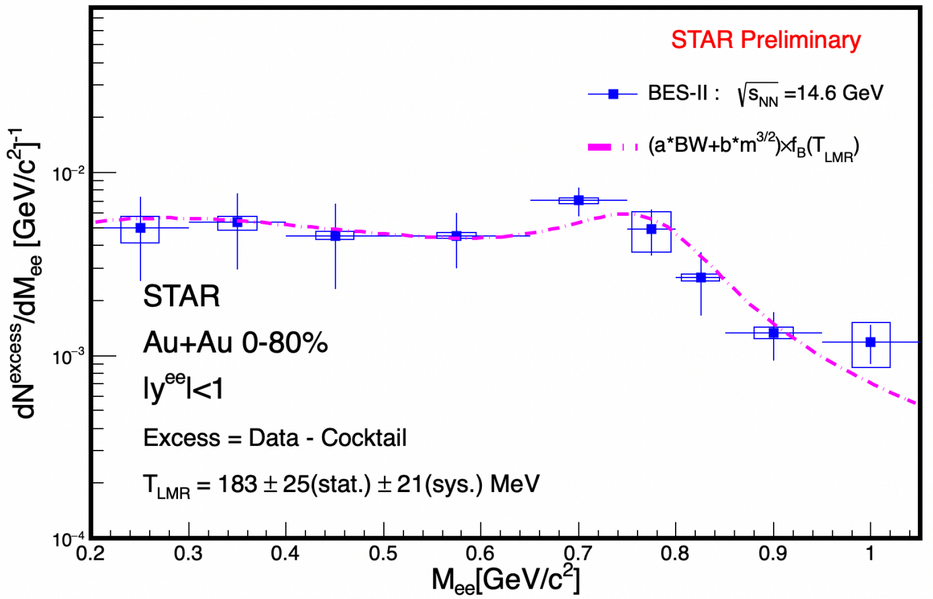

Summary of temperature measurement

- LMR:
  - T is close to both T_{ch} and T_{pc}.
  - Results indicate the LMR thermal dileptons are predominantly emitted at a later stage of the medium evolution around the phase transition.

- IMR:
  - T is higher than both T_{ch} and T_{pc}, indicating radiation from a hotter source and providing potential evidence for QGP thermal emission.
  - Thermal dileptons mainly emitted from QGP phase.

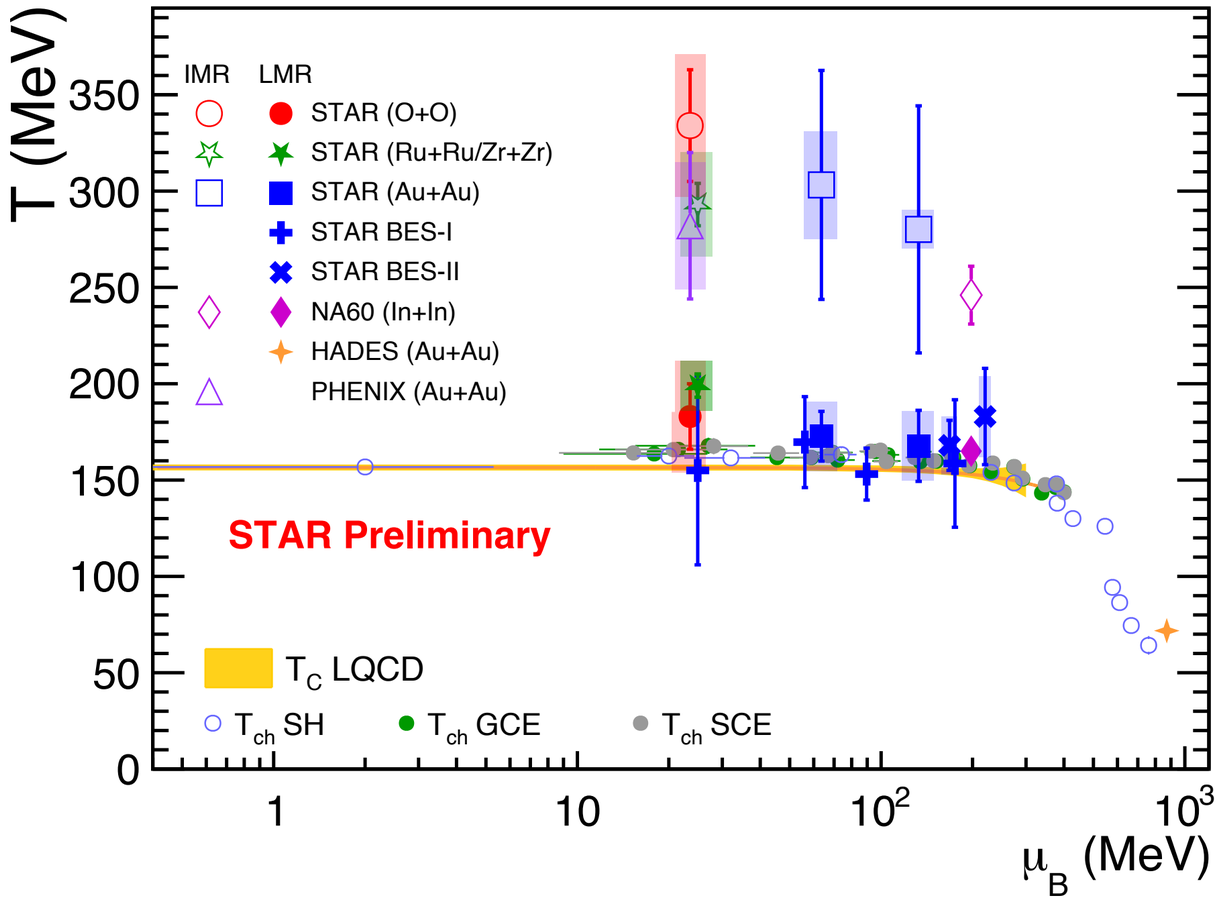

STAR: Nature Communication 16, 9098 (2025)
NA60: EPJC (2009) 59 607–623
HADES: Nature Physics 15, 1040-1045 (2019)
T. G.: JPS Conf.Proc. 32 (2020) 010079
T_{ch} SH: P. Braun-Munzinger et al. Nature 561, 321-330 (2018)
T_{ch} GCE/SCE: STAR Phys. Rev. C 96, 044904 (2017)

Dileptons as conductivity meter

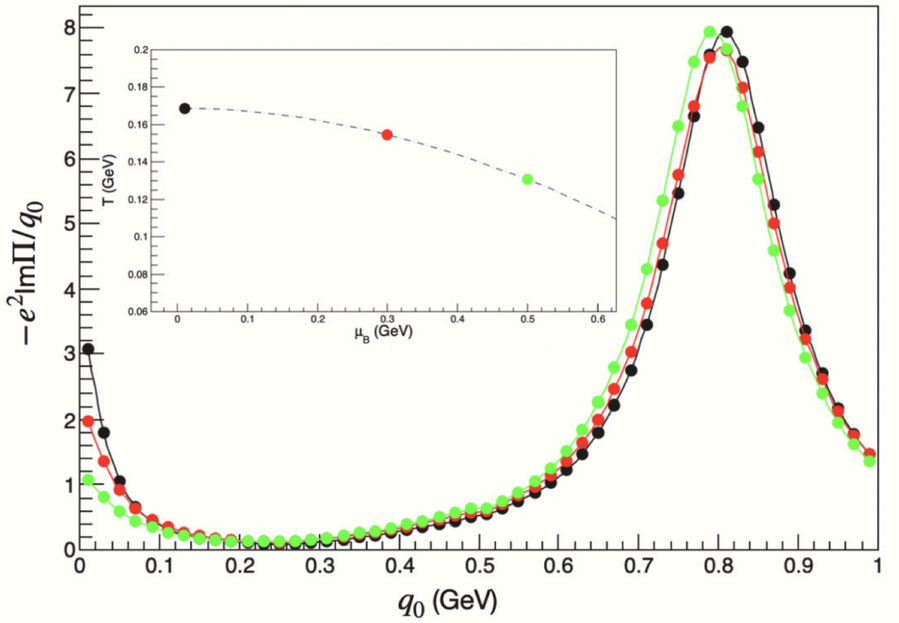

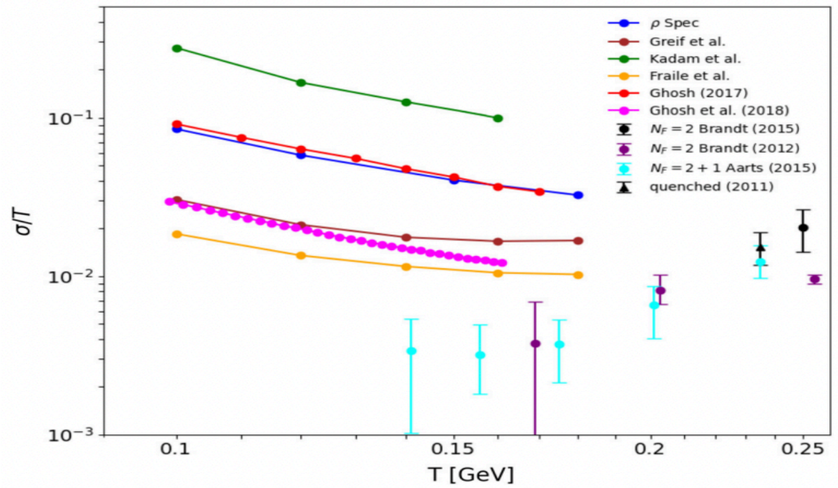

In the zero-momentum, low energy limitation, Electrical Conductivity:

Moore & Robert arXiv:hep-ph/0607172

$$\sigma_{\mathrm{el}} = -\frac{e^2}{3}\lim_{q_0\to 0}\frac{1}{q_0}\mathrm{Im}\left[\Pi_{\mathrm{EM}}(q_0, q=0, T)\right]$$

- At low energy limit, EM spectral function is related to electrical conductivity.
- Various theoretical estimations can be constrained via precise experimental measurements.
- Experimental challenge:
  - low invariant mass and p_T limit.
  - precise result on hadron contribution.

STAR Dielectron Acceptance

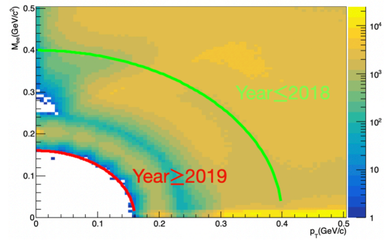

J. Atchison and R. Rapp, Nucl. Phys. A 1037, 122704 (2023)
J. Atchison, Y. Han, F. Geurts, Phys. Lett. B 858, 139024 (2024)
M. Greif, etc. Phys. Rev. D 93, 096012 (2016)

Summary

- Systematic study of dielectron invariant mass spectrum measurement at $\sqrt{s_{NN}}$ = 7.7, 9.2, 11.5, 14.6 and 19.6 GeV.
  - The data support that the ρ resonance **“melts”** into a continuum of e^+e^- pairs where the ρ meson propagator is **modified** in the medium.
  - Data agrees there is a **decreasing trend** in normalized integrated excess yield for Au+Au collisions as the collision energies decreases.

- First temperature measurement at BES-II energies.
  - 19.6 and 14.6 GeV LMR Temperature are **close** to pseudo critical temperature.
  - Summary of STAR LMR temperature results indicate the thermal radiation from hadronic gas is mainly produced **around the phase transition**.

Back Up

Collision Geometry and Centrality

M. L. Miller, K. Reygers, S. J. Sanders and p. Steinberg, 2007

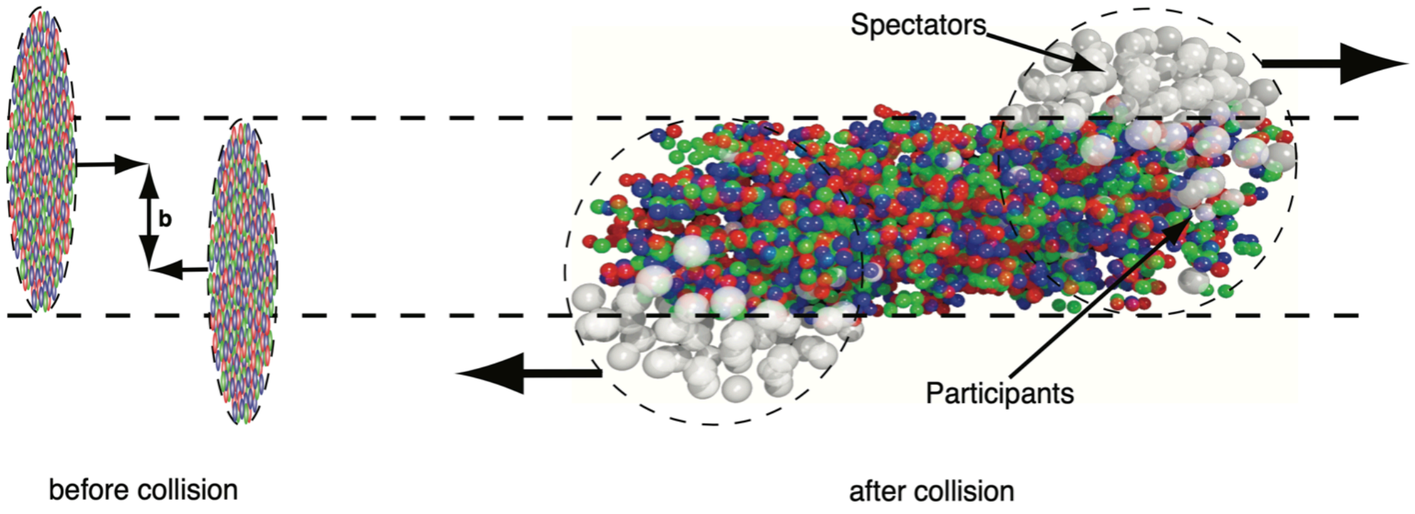

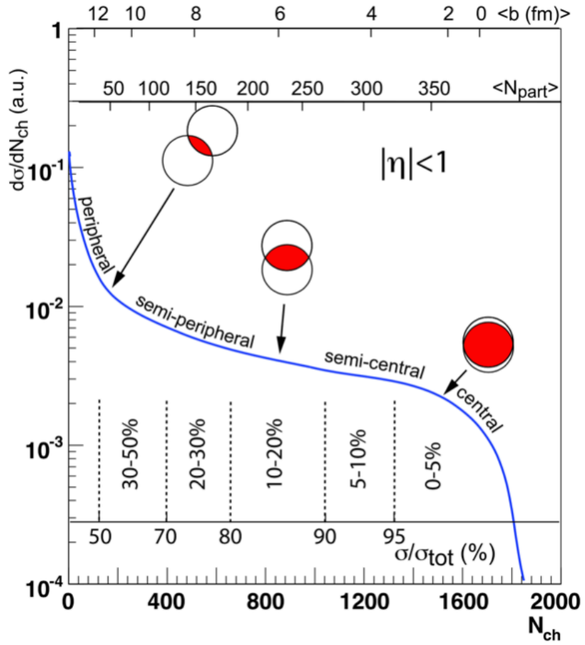

- Geometric Variables quantify Centrality:
  - Impact parameter *b*: distance between nuclei centers.
  - The number of participant nucleons: N_{part}.
  - The number of binary nucleon–nucleon collisions: N_{coll}.
- Glauber Model: geometric framework for describing nucleus–nucleus collisions.

Centrality classes are defined as percentile intervals of the observed multiplicity distribution.

Zero Degree Calorimeter

- Neutral beam fragments are detected downstream of a large-aperture accelerator dipole magnet.
  - Dipole steering magnet to separate the neutrons and protons.
  - Measure the energy deposition of neutrons.

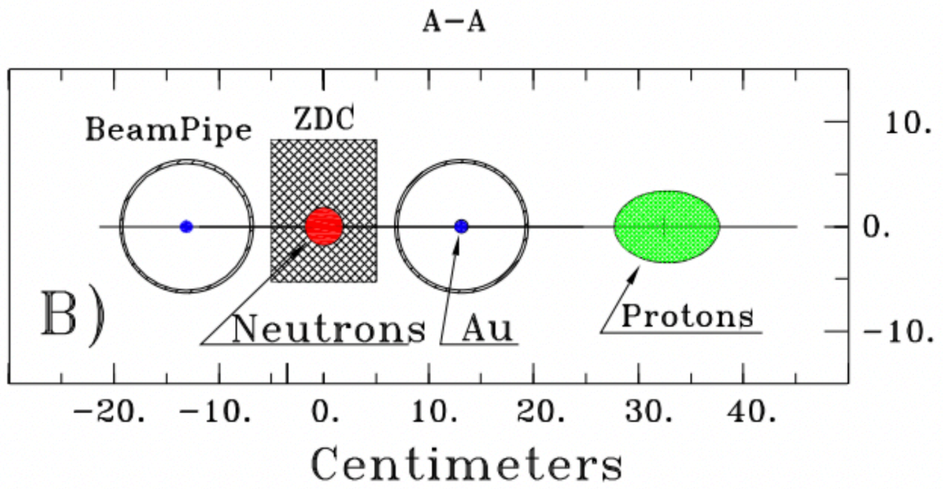

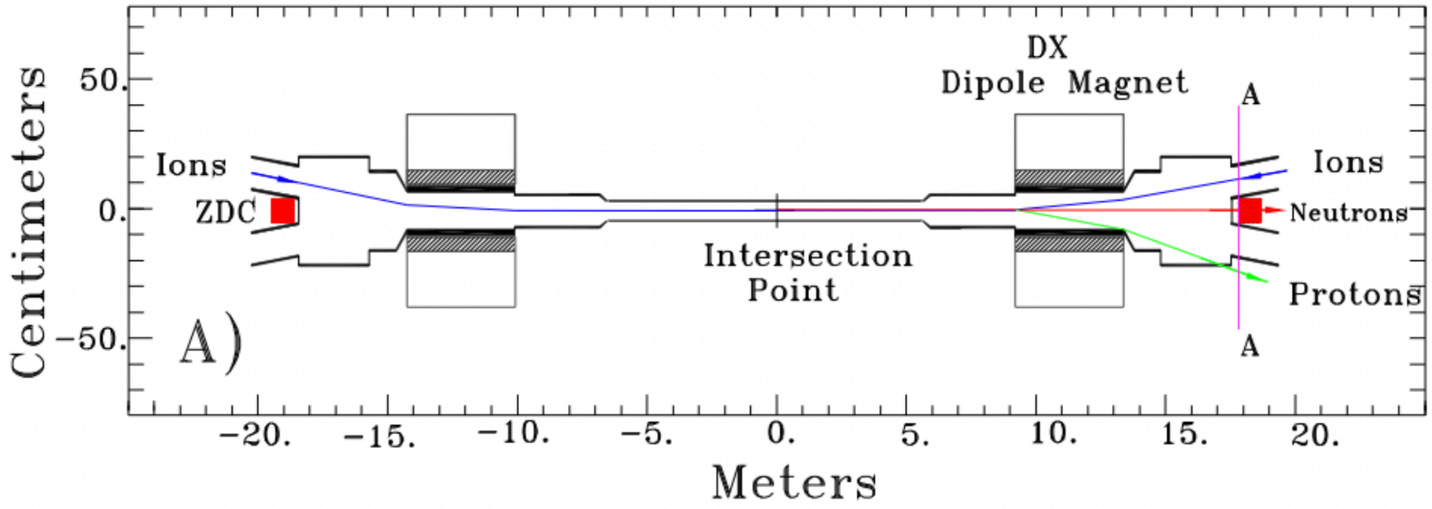

Vertex Position Detector

- Pseudo-rapidity range:
  - $4.24 < |\eta| < 5.1$.
- Pb converter + plastic scintillator + photomultiplier tube (PMT).
- Detect photons → charged particles (electrons) → visible light (scintillation process) → fast node electric pulse (PMT converts).
- 19 detectors per assembly each side.

$$T_{start} = \frac{T_{east} + T_{west}}{2} - \frac{L}{c}$$

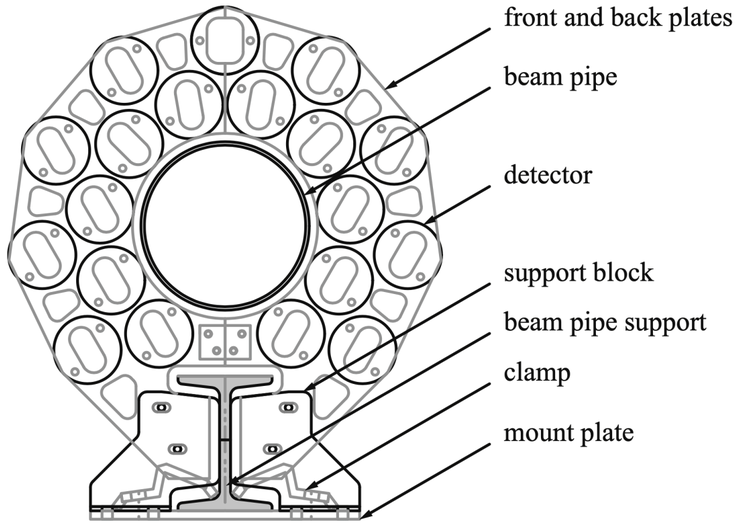

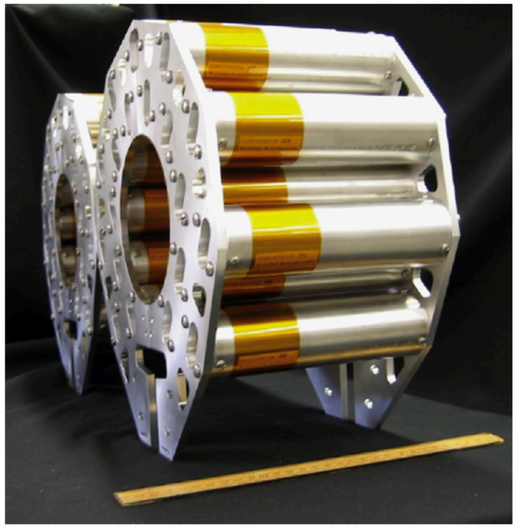

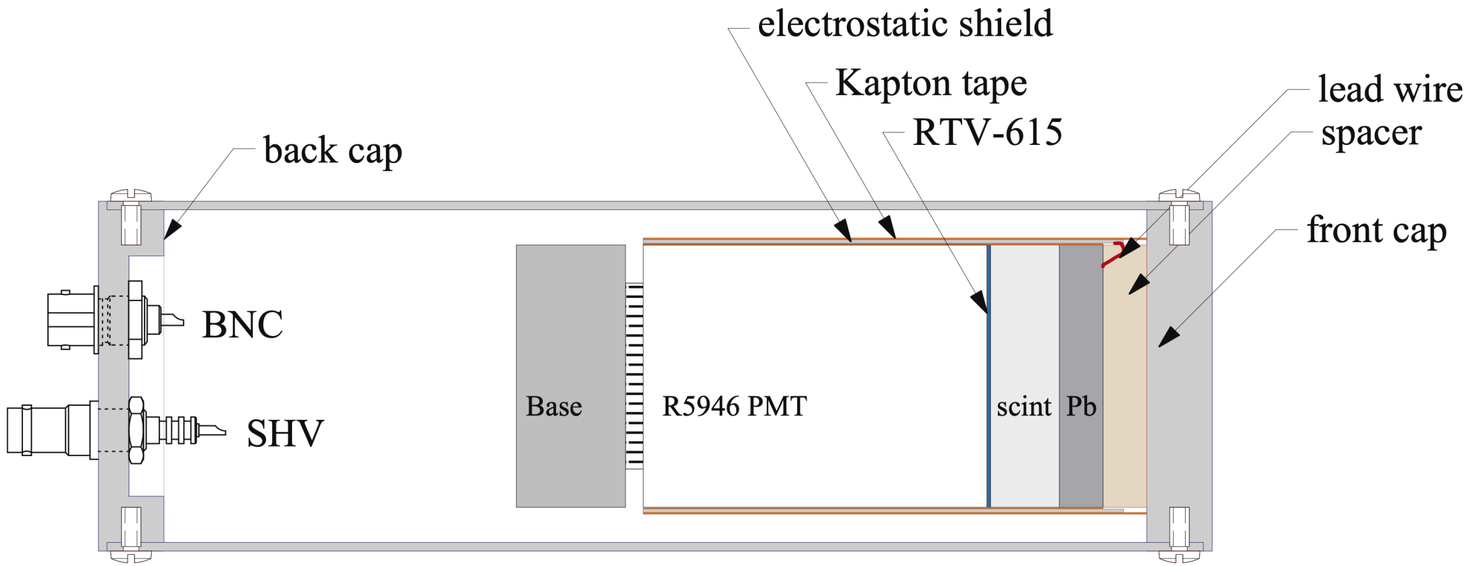

Time Projection Chamber design detail

- Signal generation procedure: Multiple-Wire Proportional Chambers (MWPC).

- Gating Grid:
  - Switching electric potential.
  - Synchronization with collision events.
  - Preventing “unwanted” electrons.

- Ground Grid:
  - Maintaining uniform and stable electric field.

- Anode Grid:
  - Accelerate electrons.
  - Townsend avalanche.

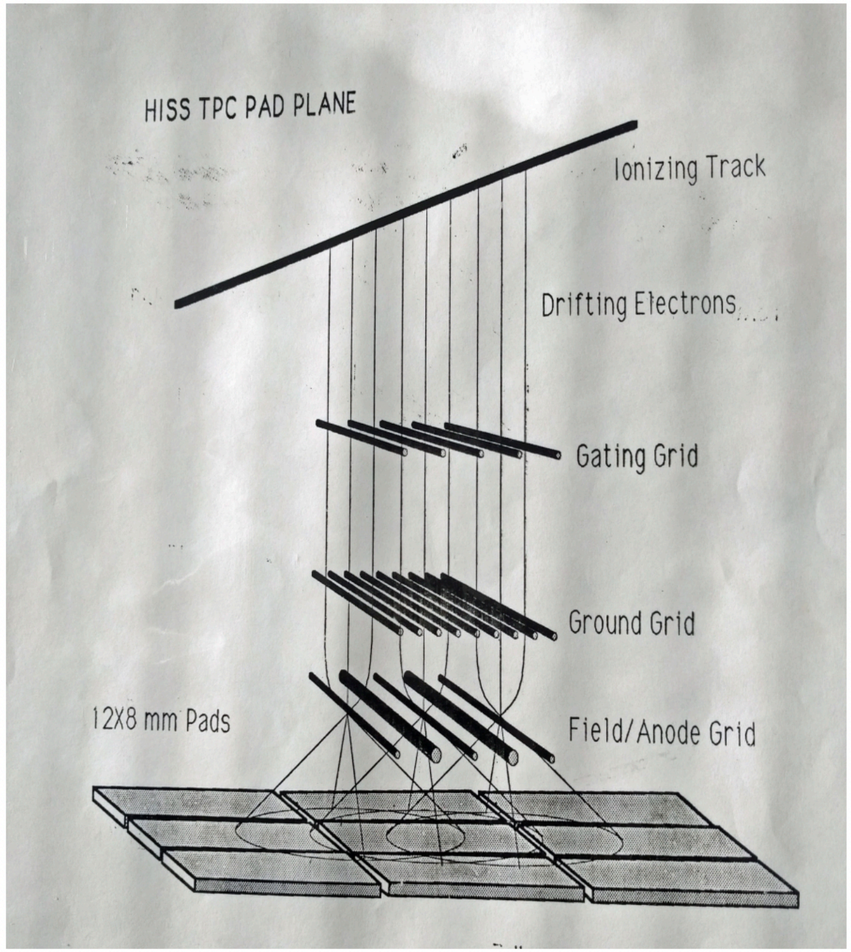

H. Wieman Nuclear Physics A 525 (1991) 617- 620

Time Projection Chamber design detail

STAR Conceptual Design Report, 1992

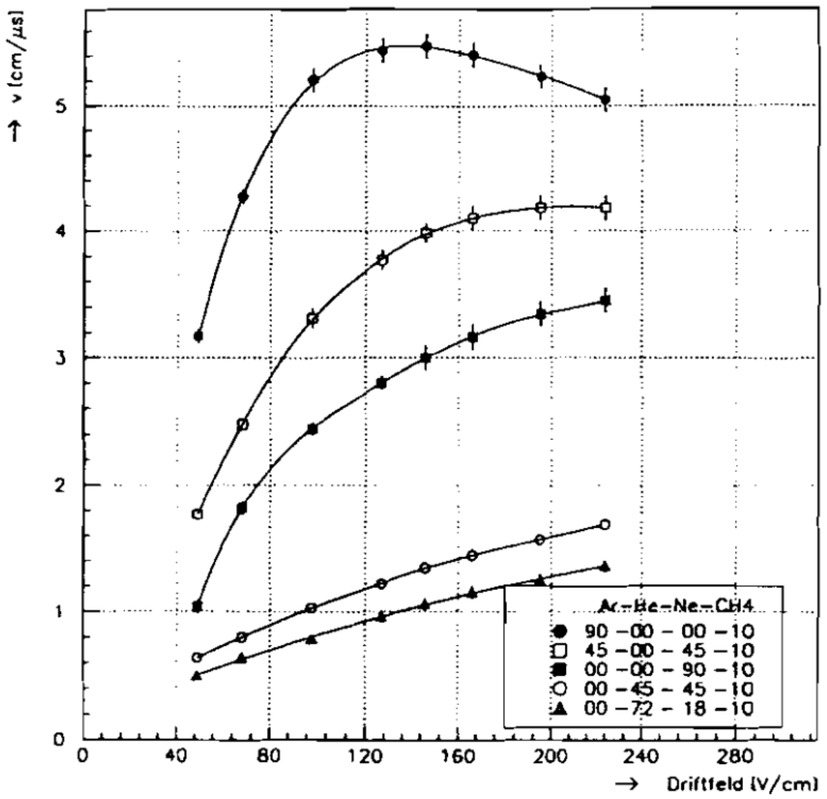

Drift velocity as a function of electric field. Deciding field strength as the peak of drift velocity.

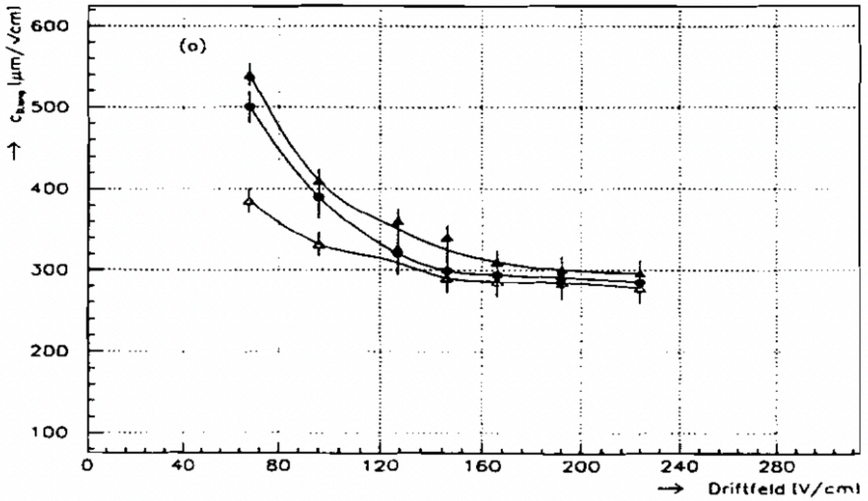

Longitudinal diffusion as a function of drift field. Deciding field strength as the lowest point of diffusion.

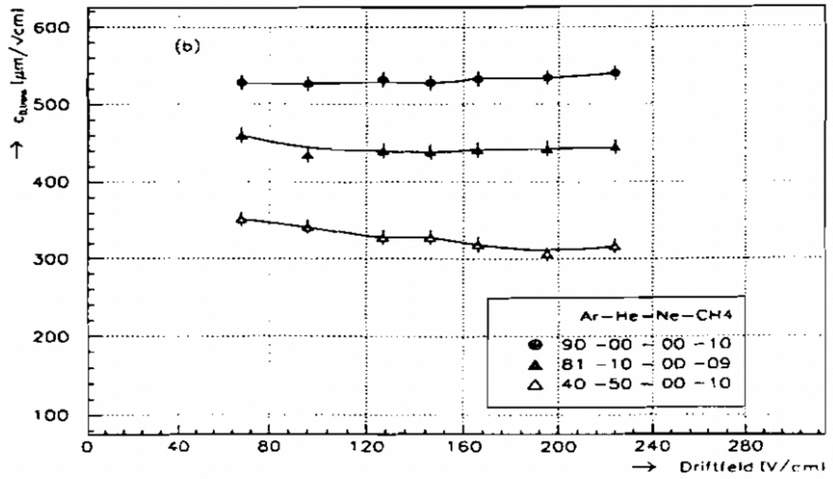

Transverse diffusion as a function of drift field. Deciding field strength as the lowest point of diffusion.

Time Projection Chamber design detail

STAR Conceptual Design Report, 1992

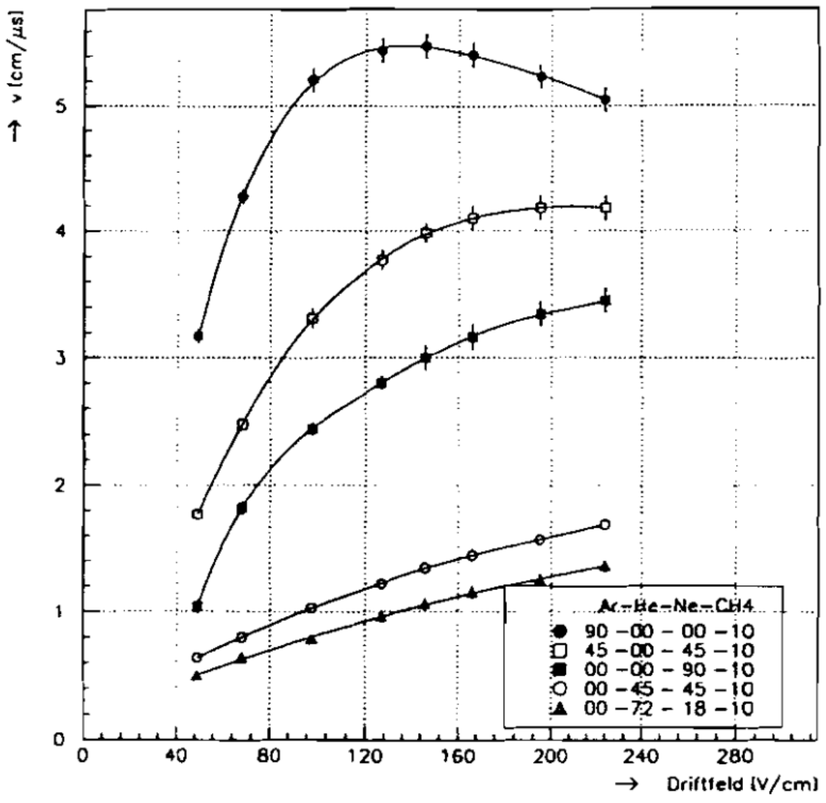

Drift velocity as a function of electric field. Deciding field strength as the peak of drift velocity.

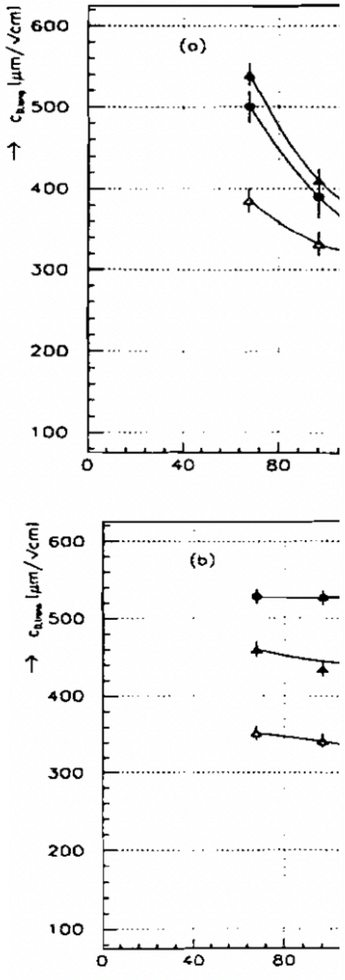

Item	Dimension	Comment
Length of the TPC	420 cm	Two halves, 210 cm long
Outer Diameter of the Drift Volume	400 cm	200 cm radius
Inner Diameter of the Drift Volume	100 cm	50 cm radius
Distance: Cathode to Ground Plane	209.3 cm	Each side
Cathode	400 cm diameter	At the center of the TPC
Cathode Potential	28 kV	Typical
Drift Gas	P10	10% methane, 90% argon
Pressure	Atmospheric + 2 mbar	Regulated at 2 mbar above Atm.
Drift Velocity	5.45 cm / μs	Typical
Transverse Diffusion (σ)	$230\mu m/\sqrt{cm}$	140 V/cm & 0.5 T
Longitudinal Diffusion (σ)	$360\mu m/\sqrt{cm}$	140 V/cm
Number of Anode Sectors	24	12 per end
Number of Pads	136,608	
Signal to Noise Ratio	20 : 1	
Electronics Shaping Time	180 ns	FWHM
Signal Dynamic Range	10 bits	
Sampling Rate	9.4 MHz	
Sampling Depth	512 time buckets	380 time buckets typical
Magnetic Field	0, $\pm$0.25 T, $\pm$0.5 T	Solenoidal

STAR PID system: Time Projection Chamber (TPC)

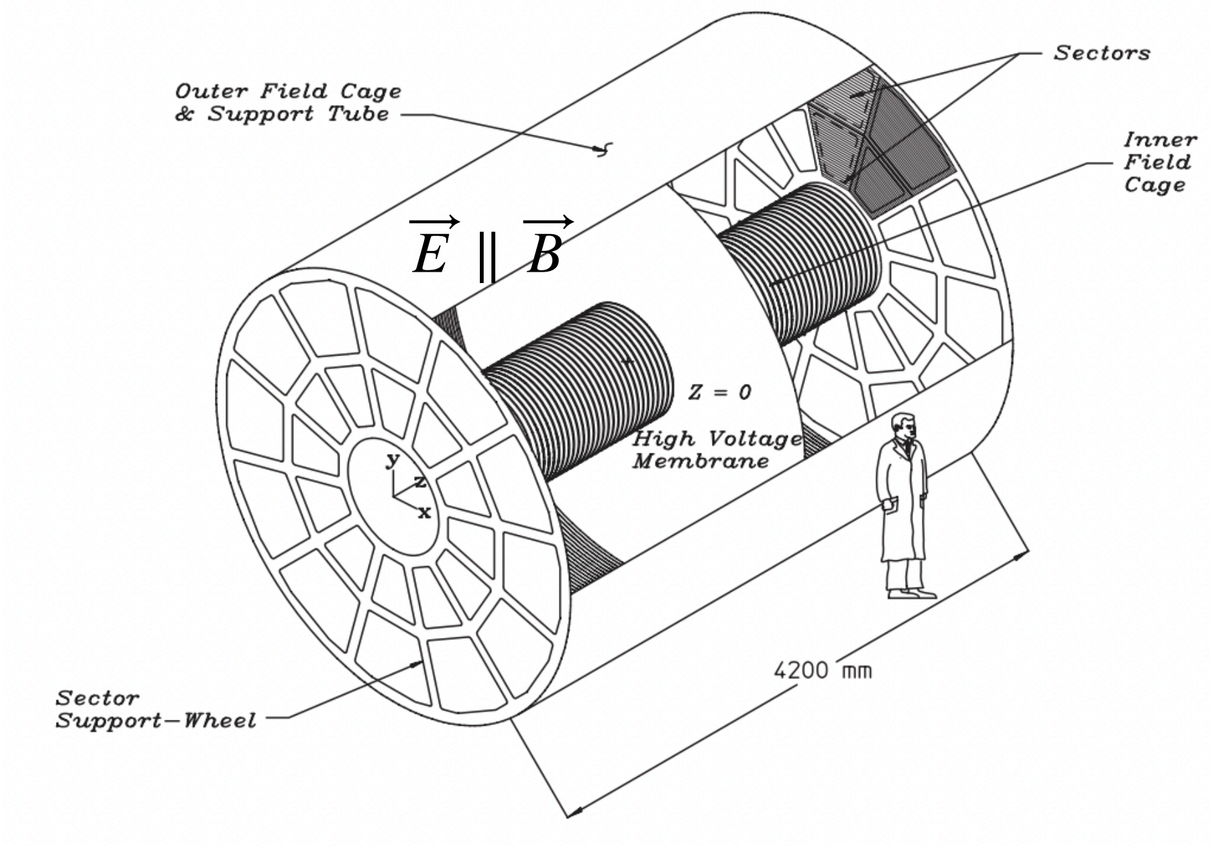

- STAR TPC is a cylinder gas detector.
  - TPC gas: 90% argon, 10% methane.
- Field cage: uniform electric field (135 V/cm), drift velocity ~5.5 cm/μs .
- Solenoidal magnetic: uniform magnetic field (0.5 T).
- Charge particles ionize gas:
  - Electric field drift electrons to anode end (connect to readout pad).

M. Anderson, et al., Nucl. Instrum. Meth. A499:659-678,2003

STAR PID system: Time Projection Chamber (TPC)

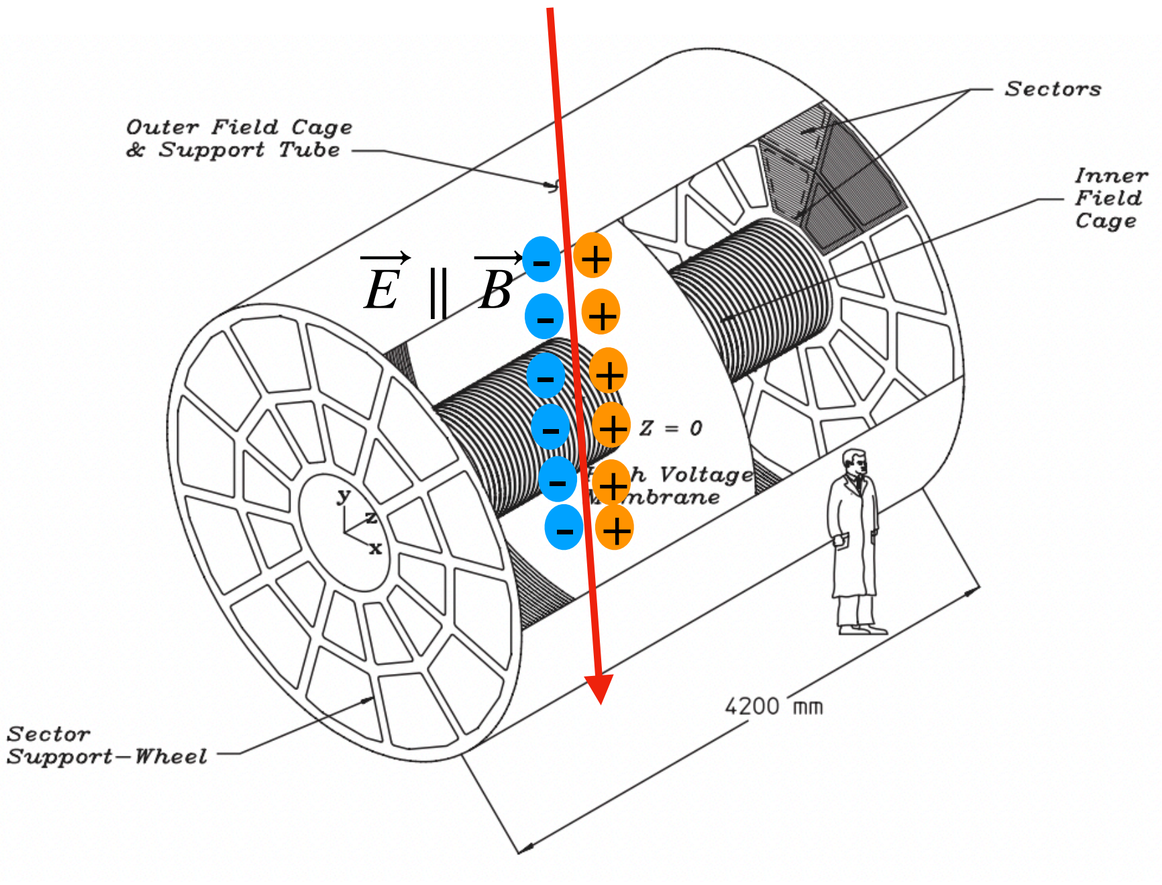

M. Anderson, et al., Nucl. Instrum. Meth. A499:659-678,2003

- STAR TPC is a cylinder gas detector.
  - TPC gas: 90% argon, 10% methane.
- Field cage: uniform electric field (135 V/cm), drift velocity ~5.5 cm/μs .
- Solenoidal magnetic: uniform magnetic field (0.5 T).
- Charge particles ionize gas:
  - Electric field drift electrons to anode end (connect to readout pad).
- Particle trajectory 3D position.
- Ionization energy loss (dE/dx).
- Momentum information.

STAR PID system: Time Projection Chamber (TPC)

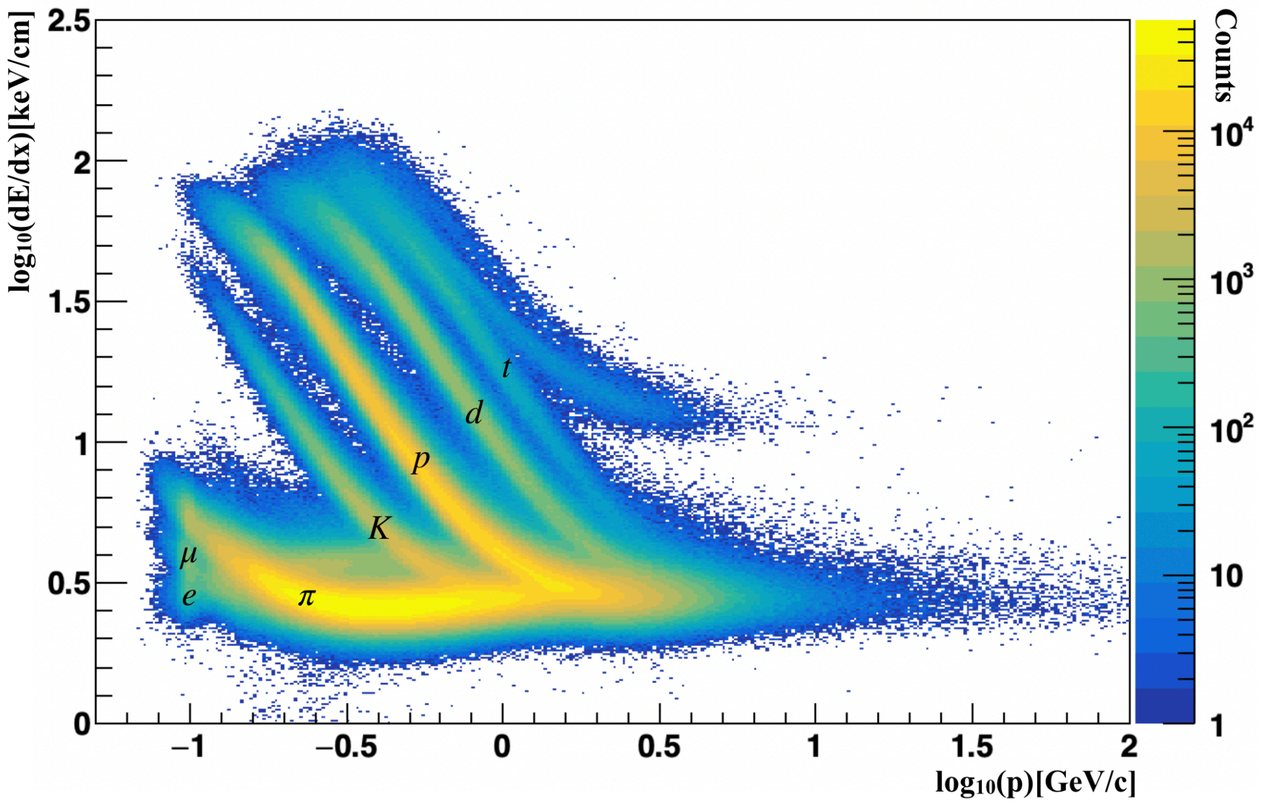

- STAR TPC is a cylinder gas detector.
  - TPC gas: 90% argon, 10% methane.
- Field cage: uniform electric field (135 V/cm), drift velocity ~5.5 cm/μs .
- Solenoidal magnetic: uniform magnetic field (0.5 T).
- Charge particles ionize gas:
  - Electric field drift electrons to anode end (connect to readout pad).

- Particle trajectory 3D position.
- Ionization energy loss (dE/dx).
- Momentum information.

STAR PID system: Time-of-Flight (TOF) system

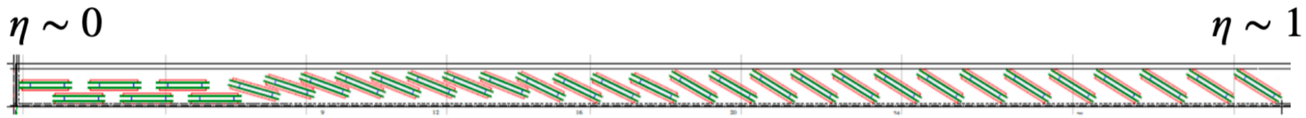

Barrel Time-Of-Flight Detector (BTOF)

- Positioned outside the TPC at a radius of 210 cm.
- 120 identical trays, 60 on the east and 60 on the west.
- Nearly 2π azimuthal coverage with narrow gaps.

- Consist of Multi-Gap Resistive Plate Chamber (MRPC).
  - composed of 95% Freon R134a (ionizing) and 5% isobutane (quenching).
- Decide the “trajectory end time” t_1. Resolution ~ 80ps.

Vertex Position Detector (VPD)

- Pb convertor + scintillator + PMT
- VPDstart Mode: measure “event initial time” t_0.

Crispin Williams, 2011 CERN Detector Seminar

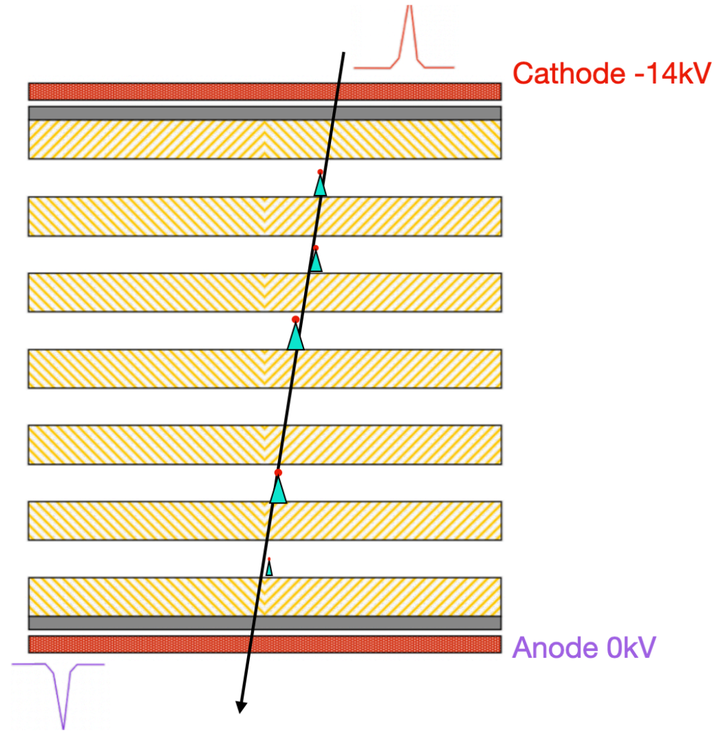

STAR PID system: Time-of-Flight (TOF) system

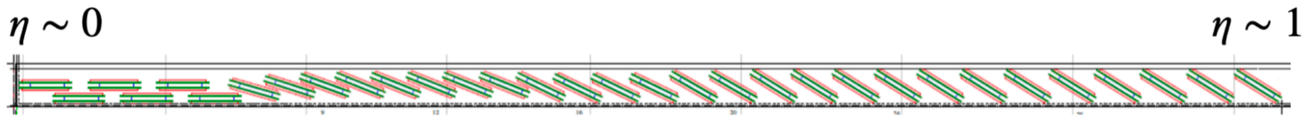

Barrel Time-Of-Flight Detector (BTOF)

- Positioned outside the TPC at a radius of 210 cm.
- 120 identical trays, 60 on the east and 60 on the west.
- Nearly 2π azimuthal coverage with narrow gaps.

- Consist of Multi-Gap Resistive Plate Chamber (MRPC).
  - composed of 95% Freon R134a (ionizing) and 5% isobutane (quenching).
- Decide the “trajectory end time” t_1. Resolution ~ 80ps.

Time of Flight = t_1 - t_0.

- Particle velocity and mass determination via combination with TPC momentum measurement.

Particle multiplicity limitation in VPD at lower collision energies.

- Startless Mode: initial time t_0. calculated based on the average time of flight with TPC measurement.

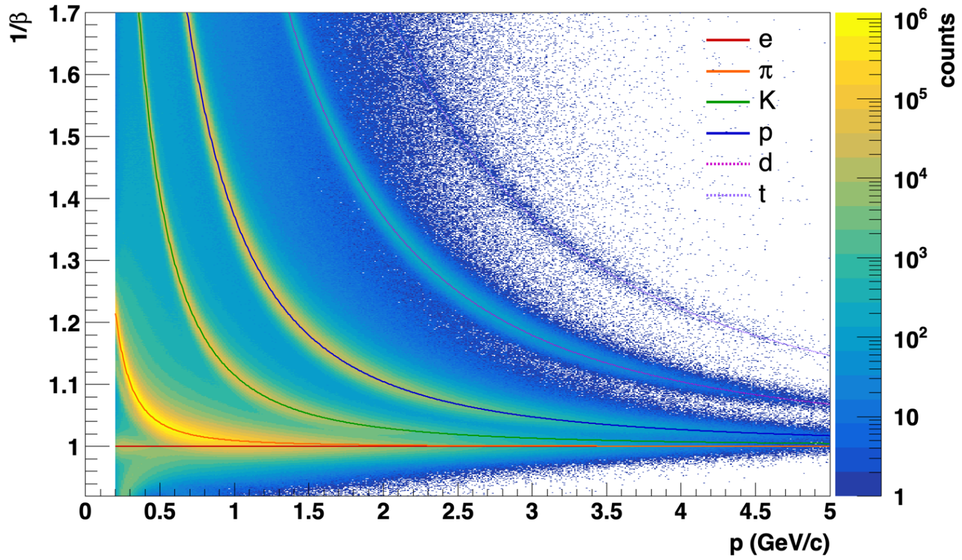

Analysis information: event selection

- Dataset: Run17 54.4 GeV, Run18 27 GeV.
- Trigger: minbias (Centrality 0-80%)
- Badrun list: STAR official QA group badrun list.
- Event pile-up rejection via RefMult vs nTofMatch cut.
- $|V_z| < 35$cm
- $|V_r| < 2$cm

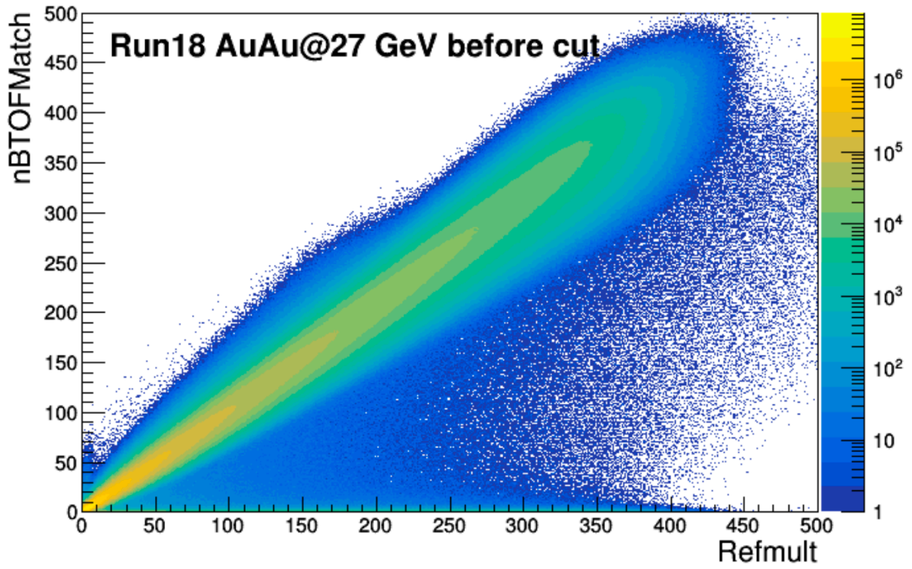

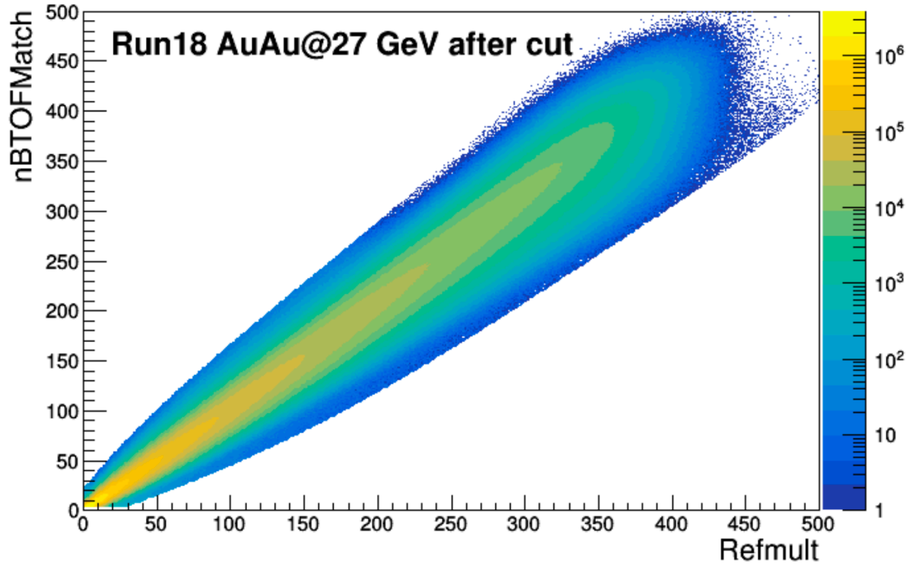

Event Plane angle correction

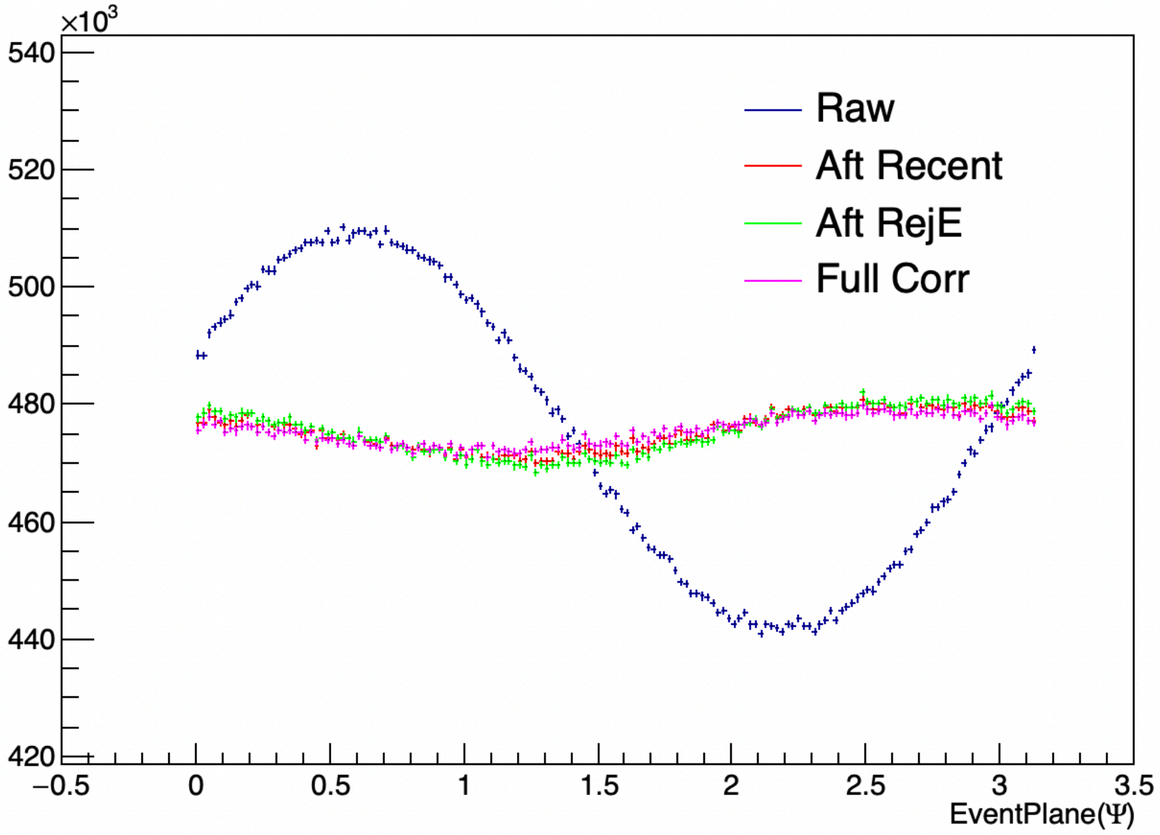

- Raw event plane angle:

$$q_x^0 = cos(2\phi) * p_T,\ q_y^0 = sin(2\phi) * p_T$$

$$Q_x^0 = \sum_{itrk} q_x^0[itrk],\ Q_y^0 = \sum_{itrk} q_y^0[itrk],\ \Psi_0 = 0.5 \times arctan(\frac{Q_y^0}{Q_x^0})$$

- Recenter Correction:

$$q_x^1 = q_x^0 - \left\langle q_x^0 \right\rangle,\ q_y^1 = q_y^0 - \left\langle q_y^0 \right\rangle$$

$$Q_x^1 = \sum_{itrk} q_x^1[itrk],\ Q_y^1 = \sum_{itrk} q_y^1[itrk],\ \Psi_1 = 0.5 \times arctan(\frac{Q_y^1}{Q_x^1})$$

- Reject electrons from event to remove the correlation between signal and reference.

- Event by event Correction:

$$n\Delta\Psi_n = \sum_{i=1}^{21} \frac{2}{i}(-\left\langle sin(in\Psi_1) \right\rangle cos(in\Psi_1) + \left\langle cos(in\Psi_1) \right\rangle sin(in\Psi_1))$$

Analysis procedure

- Dielectron pair raw signal:
  - Photonic electron removal.
  - Raw Signal = Same Event Unlike-Sign - Same Event Geometric Like-Sign × PSAC

- Efficiency correction: Pair efficiency from MC simulation.

- Hadronic cocktail: MC simulation
  - Meson decay: π , η, ω, φ, η', J/ψ
  - Semi-leptonic decay of correlated charm and Drell-Yan.

Pair Acceptance Correction Factor (PSAC)

$$S_{+-} = N_{+-} - 2\sqrt{N_{++}N_{--}} \cdot \left(\frac{B_{+-}}{2\sqrt{B_{++}B_{--}}}\right)$$

"**N**": from same event,
"**B**": from mixed event

S_{+-} —efficiency correction→ S_{corr} —subtract hadronic cocktail→ Excess Yield

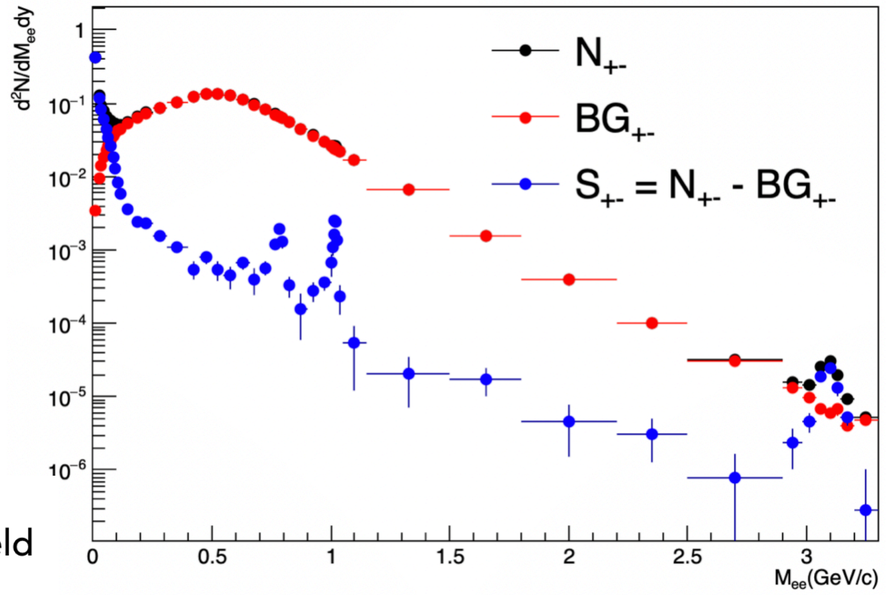

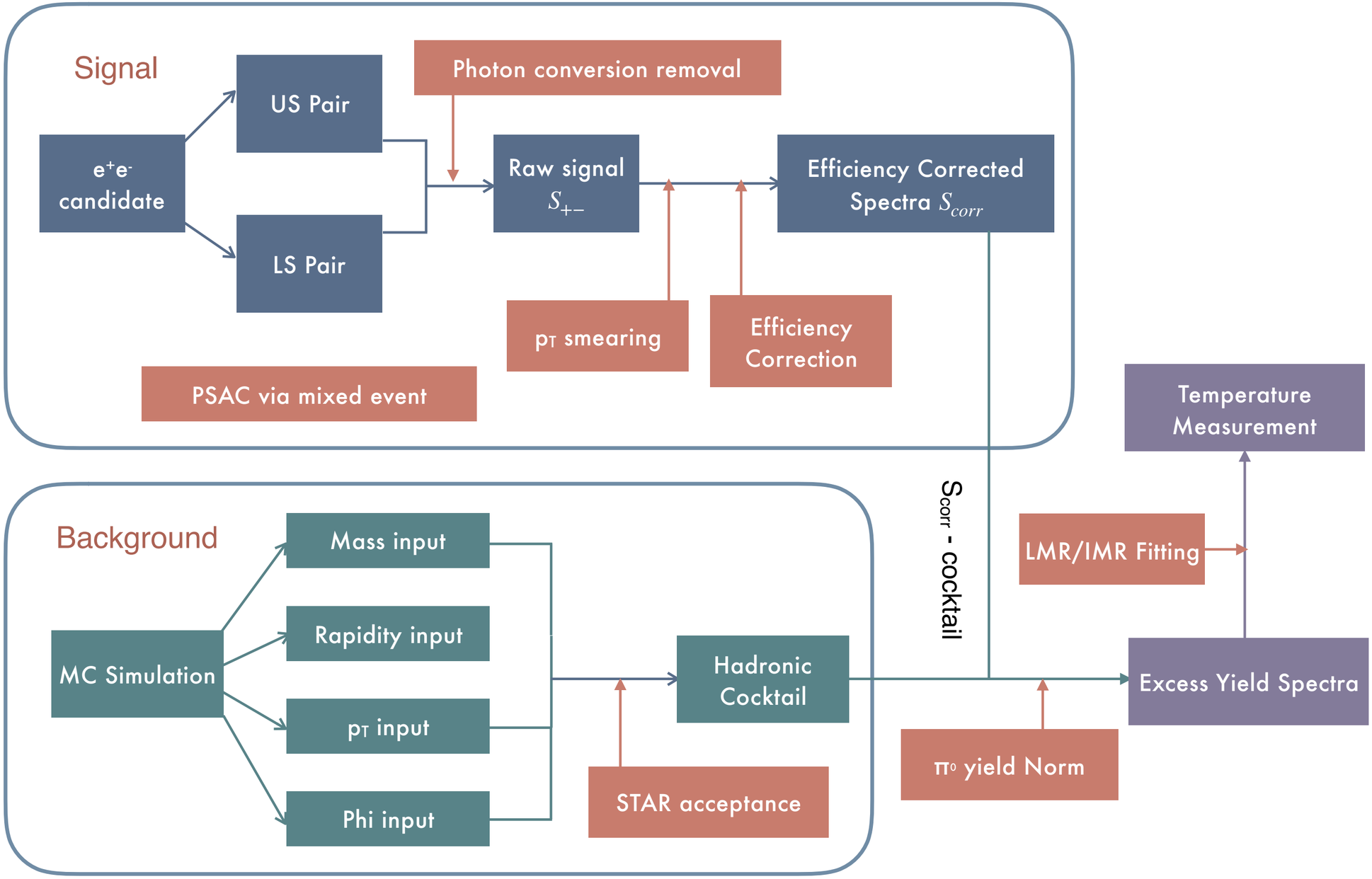
Signal
US Pair
e+e- candidate
LS Pair
Photon conversion removal
Raw signal S_{+-}
Efficiency Corrected Spectra S_{corr}
pT smearing
Efficiency Correction
PSAC via mixed event
Background
Mass input
Rapidity input
MC Simulation
pT input
Phi input
Hadronic Cocktail
STAR acceptance
Scorr - cocktail
Temperature Measurement
LMR/IMR Fitting
Excess Yield Spectra
π0 yield Norm

Physical Background: Hadronic Cocktail

- MC simulation : Parent particle $\rightarrow (X)e^+e^-$ in STAR detector environment.
- Dalitz Decay, Mass distribution: Kroll-Wada.
  - $\omega \rightarrow \pi^0 e^+e^-, \phi \rightarrow \eta e^+e^-$
  - $M \rightarrow \gamma e^+e^-$ $(M : \pi^0, \eta, \eta')$
- Direct Decay, Mass distribution: Breit-Wigner.
  - $J/\psi \rightarrow e^+e^-$
  - $\omega \rightarrow e^+e^-, \phi \rightarrow e^+e^-$
- Parent particle p_T distribution: Tsallis Blast wave (TBW) function.
  - Fitted by experimental measurements.
- Parent particle rapidity distribution: CERES' MC event generator GENSIS.
  - Parametrized by CERES's Data
- Detector resolution and smearing effect.
  - Double crystal ball function, fitted by J/ψ data

Charmed particle pair production and Drell-Yan

- $c\bar{c}$, Drell-Yan (DY)
  - generate from PYTHIA p-p collision.
  - $D\bar{D} \rightarrow e^{-}e^{+}\nu_e\bar{\nu}_e X$: from charmed particles to dielectron.
  - $DY : q\bar{q} \rightarrow e^{+}e^{-}$: from early stage of collision.

- The total cross section for Au+Au collisions is calculated by multiplying the average number of nucleon-nucleon binary collisions (N_{coll}) for a given collision centrality.

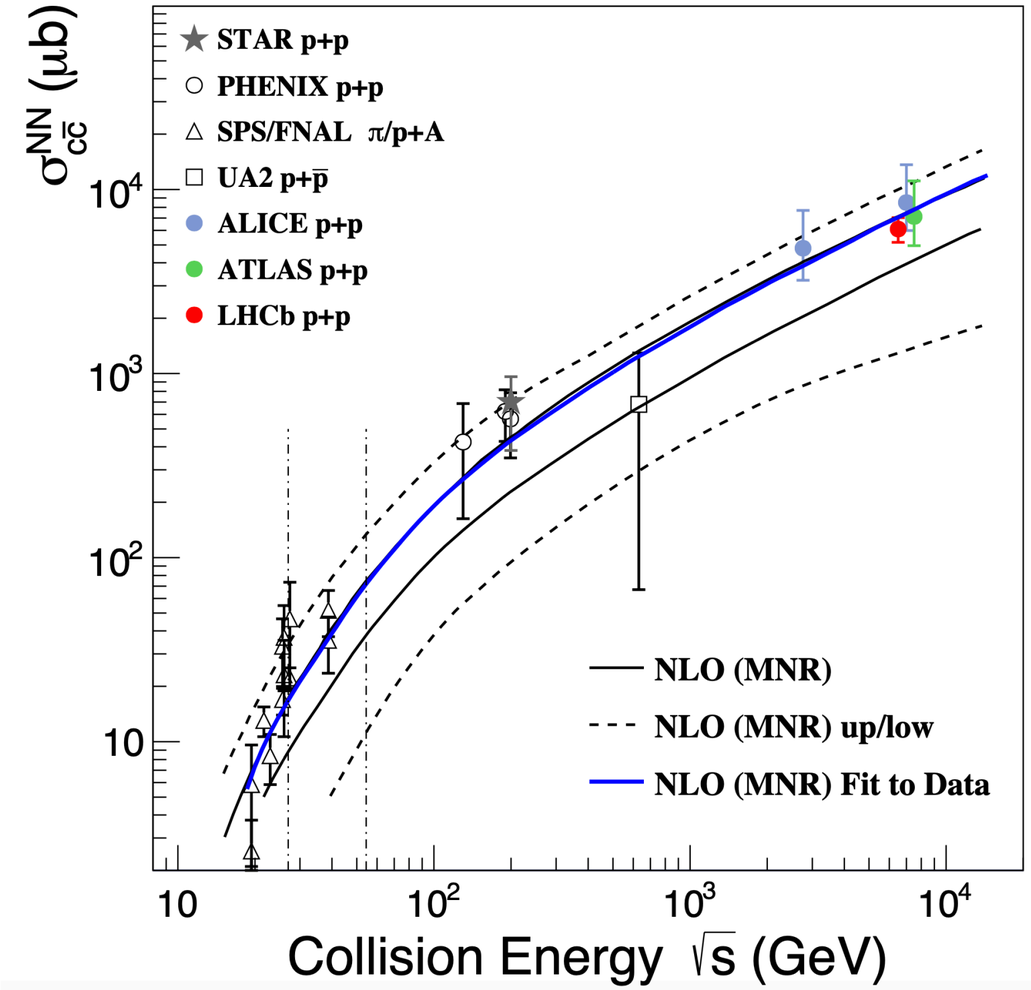

Nelson, R. E., Vogt, R. & Frawley, A. D. Phys. Rev. C 87, 014908 (2013)
Cacciari, M., Nason, P. & Vogt, R. Phys. Rev. Lett. 95, 122001 (2005)

Charmed Particle Pair and Drell-Yan

- $c\bar{c}$, Drell-Yan (DY)
  - generate from PYTHIA p-p collision.
  - $D\bar{D} \rightarrow e^{-}e^{+}\nu_e\bar{\nu}_e X$: from charmed particles to di-electron
  - $DY : q\bar{q} \rightarrow e^{+}e^{-}$: from early stage of collision

$\sqrt{s}$ (GeV)	$\sigma_{c\bar{c}}$ (μb) from NLO curve fit ($\sqrt{s}$ <= RHIC)	$\sigma_{c\bar{c}}$ (μb) from FONLL
27	17.47	17.30
54.4	75.26	74.81

PYTHIA Setting	**Purpose**
MSEL(1)	Enables minimum-bias event generation.
PARP(91, 1.0)	Specifies the width of the Gaussian primordial transverse momentum (k_T) distribution of partons inside the hadron.
PARP(67, 1.0)	Defines a scaling factor applied to the squared momentum transfer Q^2 in hard scattering processes, which controls the effective hardness of the simulated interaction.

PYTHIA Setting	**Purpose**
MSEL(11) & MSTP(43,1)	Enable the production of Z^0 and γ^* bosons.
MSTP(32,4)	Specify the production mechanism as quark–antiquark annihilation.
PARP(91,1.0)	Set the width of the Gaussian primordial transverse momentum (k_T) distribution for partons inside hadrons.
MDME(174–189,1)=0	Disable heavy-flavor decay channels.
MDME(182,1)=1	Enable the dielectron decay channel.

Hadronic Cocktail: Scaling

Scaling: $\frac{1}{N_{\text{evt}}}\frac{dN}{dM} = \frac{1}{N_{\text{evt}}}\left(\frac{dN}{dY}\right)_{\pi^0} \Delta Y \frac{\sigma_{\text{had}}}{\sigma_{\pi^0}} BR_{\text{had}\to(X)e^+e^-} \left.\frac{dN}{dM}\right|_{\text{MC, hadron}}$

$\left(\frac{dN}{dY}\right)_{\pi^0}$: neutral pion yield at mid-rapidity, adopted from experimental measurements.

$BR_{\text{had}\to(X)e^+e^-}$: Branching ratio for decay channel, PDG data.

$\frac{\sigma_{\text{had}}}{\sigma_{\pi^0}}$: cross-section ratio between π^0 and hadron.

From dielectron temperature to initial temperature

- First estimate of NLO QGP dilepton emission with finite μ_B, using hydrodynamics.
- Theoretical calculations agree with STAR BES-I data in the IMR within uncertainties.
- Potential correlation between the effective temperature extracted from IMR and the initial temperature in the fluid dynamical model to reflect different stage of the collision.

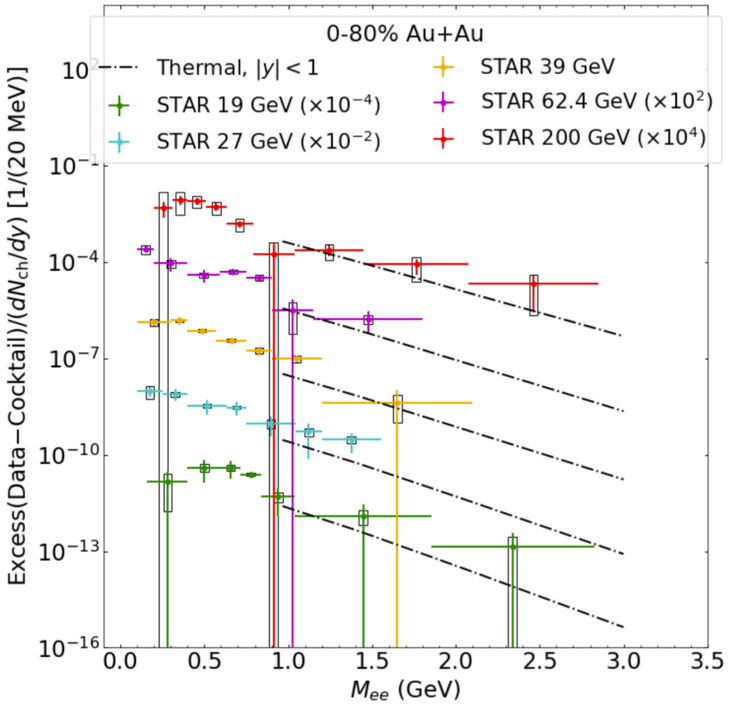

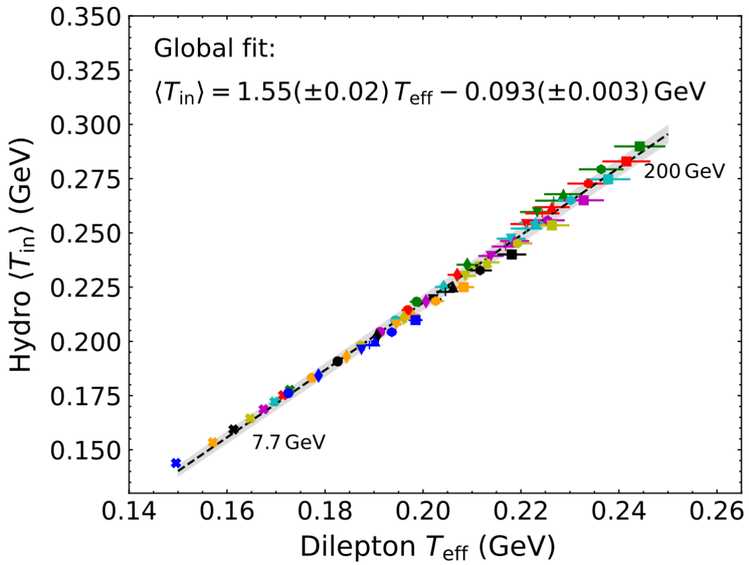

C. Gale, Quark Matter, Houston (2023)
Abhdulhamid et al. (STAR), Phys. Rev. C (2023)
J. Churchill, L. Du, C. Gale, G. Jackson, S. Jeon (2023), 2311.06675,2311.06951
A. Elfner et al., HP (2023)
B. A. Schäfer et al., Phys. Rev. C (2022)

$\langle T_{in} \rangle$: initial temperature refers to the temperature at the beginning of QGP fireball hydrodynamic expansion.